DOT/FAA/TC-12/17

Federal Aviation Administration
William J. Hughes Technical Center
Aviation Research Division
Atlantic City International Airport
New Jersey 08405

Development and Assessment of Simplified Stress Sequences for Fuselage Structures

February 2014

Final Report

This document is available to the U.S. public through the National Technical Information Services (NTIS), Springfield, Virginia 22161.

This document is also available from the Federal Aviation Administration William J. Hughes Technical Center at actlibrary.tc.faa.gov.

U.S. Department of Transportation
Federal Aviation Administration

NOTICE

This document is disseminated under the sponsorship of the U.S. Department of Transportation in the interest of information exchange. The U.S. Government assumes no liability for the contents or use thereof. The U.S. Government does not endorse products or manufacturers. Trade or manufacturers' names appear herein solely because they are considered essential to the objective of this report. The findings and conclusions in this report are those of the author(s) and do not necessarily represent the views of the funding agency. This document does not constitute FAA policy. Consult the FAA sponsoring organization listed on the Technical Documentation page as to its use.

This report is available at the Federal Aviation Administration William J. Hughes Technical Center's Full-Text Technical Reports page: actlibrary.tc.faa.gov in Adobe Acrobat portable document format (PDF).

Technical Report Documentation Page

1. Report No.	2. Government Accession No.	3. Recipient's Catalog No.
DOT/FAA/TC-12/17		
4. Title and Subtitle: DEVELOPMENT AND ASSESSMENT OF SIMPLIFIED STRESS SEQUENCES FOR FUSELAGE STRUCTURES		5. Report Date: February 2014 6. Performing Organization Code
7. Author(s): Todd Jones, John W. Rustenburg, Donald A. Skinn, and Daniel O. Tipps		8. Performing Organization Report No.
9. Performing Organization Name and Address: University of Dayton Research Institute Structural Integrity Division 300 College Park Dayton, OH 45469-0120		10. Work Unit No. (TRAIS) 11. Contract or Grant No.: Grant No. 05-G-010
12. Sponsoring Agency Name and Address: U.S. Department of Transportation Federal Aviation Administration Northwest Mountain Region – Transport Airplane Directorate 1601 Lind Avenue, SW Renton, WA 98057		13. Type of Report and Period Covered: Final Report 14. Sponsoring Agency Code: ANM-100

15. Supplementary Notes

The Federal Aviation Administration William J. Hughes Technical Center Aviation Research Division Technical Monitor was John Bakuckas. This is an update to previous draft reports.

16. Abstract

The University of Dayton Research Institute (UDRI) investigated the feasibility of using constant-amplitude stress sequences instead of comprehensive stress sequences to perform crack growth assessments of cracks located in fuselage pressure boundary structure. The goal of this effort was to determine if complex stress sequences, which account for the major flight and ground loads that a fuselage structure undergoes during operation, can be represented by a more simplified one-per-flight, constant-amplitude loading. Three different-sized airplane models that fall under Title 14 Code of Federal Regulations Part 25 were considered: a wide-body (B-777), a narrow-body (B-737), and a regional jet (Embraer ERJ-145).

The effort was divided into three tasks:

- Development of comprehensive longitudinal stress sequences at the fuselage crown above the wing for each airplane model considered—The sequences accounted for internal cabin pressure, steady-state inertia, and gust and maneuver incremental loading. The sequences were developed assuming all flights were to maximum design altitude and using published incremental vertical load factor exceedance data for the airplane models considered.
- Creation of constant-amplitude stress sequences for each airplane model with a stress ratio equal to zero and a maximum stress due to maximum design cabin pressure and steady-state inertia (i.e., 1-g flight) plus a predetermined increment of inertial loading—For this task, the same relations were used to determine the stress due to pressure and inertia loads as in task 1.
- Crack growth tests using the comprehensive sequences developed in task 1, the constant-amplitude sequences developed in task 2, and comparison of the results

Based on the data generated under task 3, the size of the airplane had a limited effect on the impact of the constant-amplitude sequence inertia increment that was added to the steady-state pressure and inertia stress. Additionally, for all three airplane models, a constant-amplitude one-per-flight cycle from zero stress to a maximum stress equal to maximum cabin pressure stress plus 1.3 times the steady-state inertia stress resulted in crack growth that was conservative when compared to crack growth due to the comparable comprehensive sequence.

Based on the work performed under this effort, it was concluded that (1) it is feasible to use a constant-amplitude stress sequence instead of a comprehensive stress sequence when assessing crack growth in fuselage pressure boundary structure, (2) a conservative estimate of crack growth will be obtained provided the constant-amplitude stress sequence used consists of one cycle per flight with a stress ratio of zero and a peak stress due to cabin pressurization plus 1.3 times the stress due to steady state inertia, and (3) conclusions 1 and 2 above are generally applicable to the fuselage pressure boundary structure of large transport airplanes.

17. Key Words	18. Distribution Statement
Fuselage, Stress sequence development, Vertical load factor, RAPID, Crack growth curve, ERJ-145, B-737-400, B-777-200	This document is available to the U.S. public through the National Technical Information Service (NTIS), Springfield, Virginia 22161. This document is also available from the Federal Aviation Administration William J. Hughes Technical Center at actlibrary.tc.faa.gov.

19. Security Classif. (of this report)	20. Security Classif. (of this page)	21. No. of Pages	22. Price
Unclassified	Unclassified	58	

Form DOT F 1700.7 (8-72) Reproduction of completed page authorized

ACKNOWLEDGEMENTS

The Flight Systems Integrity Group of the Structural Integrity Division at the University of Dayton Research Institute (URDI) performed this work under Federal Aviation Administration (FAA) Grant No. 05-G-010. Mr. James Newcomb was the Grant Technical Sponsor and Dr. John Bakuckas was the Technical Monitor for the FAA William J. Hughes Technical Center at Atlantic City International Airport, New Jersey. Mr. Daniel Tipps was the Principal Investigator for the University of Dayton and provided overall technical direction for this effort. Mr. Todd Jones created graphical presentations, documented the procedures and tests results for the final report, and completed the coupon testing with support from Mr. Greg Hartman. Mr. John Rustenburg developed the mission profiles and usage data and assisted in preparation of the report. Mr. Donald Skinn developed the data reduction algorithms and programmed the data reduction criteria and sequence algorithms.

Mr. Robert Eastin, Chief Scientific Technical Advisor on Fracture and Fatigue (retired), of the FAA and Mr. Ron Atmur, Senior Engineer of the Airframe Branch at the FAA Los Angeles Aircraft Certification Office provided technical guidance and editing support for this report.

TABLE OF CONTENTS

LIST OF FIGURES

LIST OF TABLES

LIST OF ACRONYMS

CA	Constant amplitude
CFR	Code of Federal Regulations
EDM	Electrical discharge machining
FAA	Federal Aviation Administration
MATE	Material Analysis and Testing Environment
NASA	National Aeronautics and Space Administration
OLMP	Operational Loads Monitoring Program
UDRI	University of Dayton Research Institute

EXECUTIVE SUMMARY

The University of Dayton Research Institute (UDRI) investigated the feasibility of using constant-amplitude stress sequences instead of comprehensive stress sequences to perform assessments of crack growth located in fuselage pressure boundary structure. The goal of this effort was to determine if complex stress sequences, which account for the major flight and ground loads that a fuselage structure undergoes during operation, can be represented by a more simplified one-per-flight, constant-amplitude loading. Three different sizes of transport airplanes (a wide-body (Boeing B-777) and a narrow-body model (B-737), and a regional jet (Embraer ERJ-145)), which fall under Title 14 Code of Federal Regulations (14 CFR) Part 25, were considered.

The effort was divided into three tasks:

- Development of comprehensive longitudinal stress sequences at the fuselage crown above the wing for each considered airplane model—The sequences accounted for internal cabin pressure, steady-state inertia, and gust and maneuver incremental loading. The sequences were developed assuming all flights were to maximum design altitude and using published vertical load factor exceedance data for the considered airplane models.

- Creation of constant-amplitude stress sequences for each airplane model with a stress ratio equal to zero and a maximum stress due to maximum design cabin pressure and steady-state inertia (i.e., 1-g flight) plus a predetermined increment of inertial loading—For this task, the same relations were used to determine the stress due to pressure and inertia loads as in task 1.

- Crack growth tests using the comprehensive sequences developed in task 1, the constant-amplitude sequences developed in task 2, and comparison of the results

Based on the data generated under task 3, it was observed that the size of the airplane had a limited effect on the impact of the constant-amplitude sequence inertia increment that was added to the steady-state pressure and inertia stress. Additionally, it was observed that for all three models, a constant-amplitude, one-per-flight cycle from zero stress to a maximum stress equal to maximum cabin pressure stress plus 1.3 times the steady-state inertia stress resulted in crack growth that was conservative when compared to crack growth due to the comparable comprehensive sequence.

Based on the work performed under this effort, it was concluded that

- it is feasible to use a constant-amplitude stress sequence instead of a comprehensive stress sequence when assessing crack growth in fuselage pressure boundary structure.

- a conservative estimate of crack growth will be obtained provided the constant-amplitude stress sequence used consists of one cycle per flight with a stress ratio of zero and a peak stress equal to cabin pressurization plus 1.3 times the stress due to steady-state inertia.

- conclusions 1 and 2 above are generally applicable to the fuselage pressure boundary structure of large transport airplanes.

1. BACKGROUND AND OBJECTIVE.

A large transport airplane fuselage is a pressure boundary structure that has many areas that are known to be relatively sensitive to fatigue. Because of this, damage tolerance evaluations are routinely performed on certain areas of the baseline structure (e.g., splices, window corners, door corners, and pressure bulkhead details) to support type design certification and on repairs and alterations to show compliance with the original certification basis to support compliance with the Repair Assessment for Pressurized Fuselage Rule (see Title 14 Code of Federal Regulations (CFR) 91.1505, 121.1107, 125.505, and 129.109) or to comply with the Aging Airplane Safety Rule (see 14 CFR 26.41/43/45/47/49).

To perform a crack growth evaluation, an appropriate stress sequence is required for the area and crack orientation being considered.

For those areas and cracking orientations in which relevant internal stresses are a function of cabin differential pressure only, the required stress sequence is often assumed to be a series of one-per-flight cycles; each cycle has a stress ratio of zero and the maximum stress corresponds to the maximum cabin pressure differential experienced during that flight. Further, if it is conservatively assumed that each flight is to maximum design altitude, then the required sequence is a constant-amplitude one-cycle-per-flight sequence with stress ratio equal to zero. This type of sequence is easily developed if the internal stress due to pressure is known or can be conservatively estimated.

For those areas and crack orientations in which relevant internal stresses are a function of cabin pressurization and inertia loading (e.g., fuselage bending associated with 1-g flight, maneuvers, and gust encounters), the required sequences consist of multiple cycles per flight with varying stress ratios and amplitudes. Sequence development not only requires knowledge of internal stresses due to pressurization and inertia loading but also load factor exceedances due to maneuvers and gusts. This information is used to create the required random flight-by-flight, cycle-by-cycle sequences. The sequence generation process is generally automated and beyond the typical capabilities of anyone other than the type certificate holder for a particular model airplane. Such sequences are referred to herein as "comprehensive" sequences.

The concept of using a constant-amplitude, one-cycle-per-flight sequence to approximate a comprehensive sequence is shown in figure 1 for one notional flight.

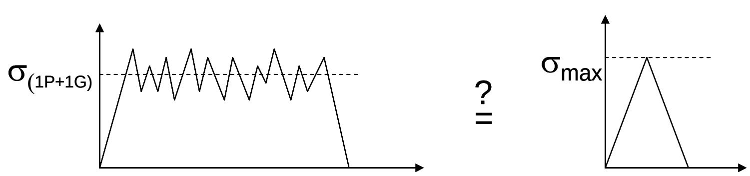

Figure 1. Equivalent One $R = 0, \quad \sigma_{max} = \sigma_{1P} + n_{ZE}\sigma_{1g}$

Use of an equivalent one-per-flight cycle is advantageous because the alternative (i.e., use of a comprehensive sequence) requires significant resources. However, to be acceptable for use, the constant-amplitude, one-cycle-per-flight sequence must result in the same crack growth or must conservatively bound the crack growth that would result from the appropriate comprehensive sequence. As shown in figure 1, the comprehensive sequence is composed of one overall ground-air-ground cycle, with a stress ratio of zero and a maximum stress equal to the stress due to maximum cabin differential pressure during the flight ($1P$) plus the stress due to 1-g inertia, onto which is superimposed incremental stresses due to maneuvers and gusts. Based on this, it can be reasonably assumed that an equivalent one-per-flight cycle would have a stress ratio of zero and a maximum stress at least equal to the $1P + 1g$ steady-state flight stress in the comprehensive sequence. However, the multiple incremental cycles in the comprehensive sequence will also contribute to crack growth, therefore, it is reasonable to expect that the constant-amplitude sequence maximum stress will need to be somewhat greater than the $1P + 1g$ level.

The primary objective of this report is to determine what the "equivalent load factor" (n_{ZE}) should be for a constant-amplitude sequence to result in equal or conservative-bounding crack growth when compared to what the appropriate comprehensive sequence would result in. In the past, n_{ZE} values ranging from 1.3 to 2.5 have been used. These values were based primarily on engineering judgment, and it was decided to perform a more quantitative evaluation of what n_{ZE} should be. A secondary objective was to determine an approach that would allow any conclusions to be generally applicable to crack growth evaluations in a large transport fuselage pressure boundary structure.

2. APPROACH.

Three different large transport airplane models were considered (a wide-body, a narrow-body, and a regional jet) to determine how much the size of the airplane affected the value of n_{ZE} needed to achieve crack growth equivalency.

Circumferential cracking in the fuselage skin at the crown of the fuselage, directly above the wing front spar, was the scenario addressed. The fuselage skin was chosen because credible and conservative estimates of skin stress due to cabin pressurization and inertia can be made in a relatively straightforward manner for any given airplane model with only a limited number of model-specific parameters (e.g., fuselage skin thickness and radius, maximum design cabin pressure differential, skin material, and design maneuver load factor). Circumferential skin cracking was chosen because the stress that must be used for a crack growth assessment includes one component due to pressure and one due to inertia. The upper crown of the fuselage above the wing front spar was chosen because the longitudinal stress in the skin is relatively high at this point and the inertia component encompasses a relatively large percentage of the total. It is believed that a value of n_{ZE} that is acceptable for this location and this crack orientation should be generally applicable for other fuselage pressure boundary structure and crack orientations.

For this cracking scenario, comprehensive sequences were developed for each large transport category airplane. Incremental vertical load factor exceedances (due to maneuvers and gusts) data were used to develop sequences. Boeing (B)-777, B-737, and Embraer Regional Jet (ERJ)-145 data, collected as part of the FAA Operational Loads Monitoring Program (OLMP), were used for the wide-body and narrow-body models and the regional jet, respectively.

For this cracking scenario, one-cycle-per-flight, constant-amplitude sequences were created for all three transport airplane categories using the same basic pressure-to-stress and inertia load-to-stress relations that were used to develop the comprehensive sequences and various values of n_{ZE}.

The crack growth resulting from each comprehensive and constant-amplitude sequence was determined experimentally, rather than analytically, to eliminate any potential effects of crack growth analysis methodology (e.g., analytical retardation model) on the outcome. Crack growth tests were performed using the comprehensive sequences and the constant-amplitude sequences. Small coupons were tested that contained center through cracks. Three coupons were tested using each sequence, and crack size was recorded as a function of number of flights.

The crack growth resulting from the comprehensive sequences and constant-amplitude sequences were compared for each transport airplane category considered and conclusions were drawn.

The general approach described above was used for all three large transport airplane categories considered. The details for the regional jet (ERJ-145) are presented in this report for example purposes.

3. DESCRIPTION OF OPERATIONAL LOADS MONITORING PROGRAM.

UDRI supports the FAA OLMP by acquiring, analyzing, and maintaining an extensive database of in-service operational usage data from various airline operators and types of airplanes. Efforts involve developing partnerships with many airline operators to acquire operational flight and ground loads usage data from the various model/type airplanes operating in routine daily service. Over 460,000 hours of operational usage data are currently in the OLMP database from the B-737-400/700, B-767, B-777-200, B-747-400, McDonnell Douglas (MD)-82/83, Airbus (A)320, A340, Beechcraft (BE)-1900D, Bombardier Canadair Regional Jet (CRJ)-100, and the ERJ-145, as shown in table 1.

Table 1. The UDRI Flight Loads Database

AirplaneType	No. of Airplanes	No. of Flights	No. of Flight Hours
B-737-400	21	62,264	91,600
B-737-700	10	3,394	6,300
MD-82/83	6	10,172	18,900
B-767-200	10	6,722	46,100
BE-1900D	28	903	585
A320	54	11,066	30,817
B-747-400	51	11,064	95,883

Table 1. The UDRI Flight Loads Database (Continued)

Airplane Type	No. of Airplanes	No. of Flights	No. of Flight Hours
CRJ-100	Fleet	467	607
B-777-200	43	10,142	67,500
A340-300	10	5,000	13,960
ERJ-145	Fleet	47,273	88,305
		Total	460,557

The flight loads parameter data received from the participating airlines are recorded by the onboard digital flight data recorder. Parameters, such as vertical, lateral, and longitudinal accelerations; gross weight; airspeed; and altitude, are recorded. Sampling rates vary from parameter to parameter and airplane to airplane. Typical sampling rates for the vertical acceleration, airspeed, and gross weight are 8 hertz, once per second, and once every 64 seconds, respectively. Additional available information about the parameters and the respective sampling rates can be found in the individual airplane OLMP Reports.

As part of the OLMP, UDRI processed and analyzed the operational flight and ground loads data, developed statistical data formats, and published statistical loads report to show how various airplane models are currently being used in operational service. These reports are currently available on the FAA William J. Hughes Technical Center library website at http://207.67.203.68/F10011Staff/OPAC/index.asp.

These reports contain data categorized as airplane usage, ground loads, and flight loads. Airplane usage data plots and tables are provided showing weights, flight distances, speeds, and altitudes. Ground loads data include lateral, longitudinal, and vertical load factor data during touchdown and ground operations, including taxi, takeoff roll, and landing roll. Flight loads data include lateral and vertical load factor data due to maneuvers and gust inputs. Maneuver and gust vertical load factor data are presented per 1000 hours or by nautical mile and by flight phase or by combined flight phases. Derived gust velocities are presented as cumulative occurrences per nautical mile versus altitude range. The OLMP statistical load reports also contain systems operational data showing flap, speed brake, and landing gear usage, and times and speeds for thrust reverser operations. All the data in UDRI database are maintained such that, at any point in time during a flight, any recorded parameter can be related to the activity of another recorded parameter or the phase of flight in which the event occurred.

3.1 PEAK-BETWEEN-MEANS COUNTING CRITERIA.

The National Aeronautics and Space Administration (NASA) was using the peak-between-means counting criteria when the FAA OLMP work was transferred to UDRI in the mid-1990s. These criteria were also recommended by de Jonge [1]. As referenced in this report, the peak-between-means criteria is well-suited to be applied in the analysis of gust-induced acceleration and is compatible with existing National Advisory Committee for Aeronautics velocity, gravity, and height gust data. UDRI has continued to use the peak-between-means counting criteria in the

OLMP because of its use in the past and the recommendation to continue to use the criteria in the future to maintain compatibility.

Following the procedures used in the NASA flight loads monitoring program [2] and de Jonge's recommendation [3], the peak-between-means counting criteria was used to count all the acceleration peaks during the OLMP. The peak-between-means counting criteria can be demonstrated best by viewing a portion of a typical vertical load factor time history trace, as shown in figure 2. The portion of the flight trace shown contains vertical acceleration peaks (P), a ±0.05-g dead band area, and a 1-g flight mean. The 1-g flight mean level is synonymous with a zero Δg value (points denoted by C in figure 2 represent a zero crossing) since the acceleration peaks are read as incremental load factors about the 1-g flight mean. The dead band applies to Δg values that are considered too small to be of consequence and are thus ignored. For example, if one starts at C_0, which is the 1-g flight mean, the first peak to consider is P_1. P_1 is counted as a positive peak because the trace moved outside of the dead band and returns to the 1-g mean at C_1. The 1-g flight mean functions as a reset to count the peak and as a starting point to begin searching again for the next peak. The next peak is P_2. This peak is counted as a negative peak because the trace returns to the mean at C_2 and resets. Peaks P_3 and P_4 are not counted because they are inside the dead band. The next point, C_4, restarts the process to look for the next peak and finds that P_5 is a peak when C_5 is crossed. Similarly, P_6 becomes a peak when C_6 is crossed, and finally P_7 becomes a peak when C_7 is crossed. This counting procedure continues on throughout a given flight until all the peaks have been counted for the entire flight. This process is then continued for each flight until all vertical acceleration peaks for that airplane model have been counted.

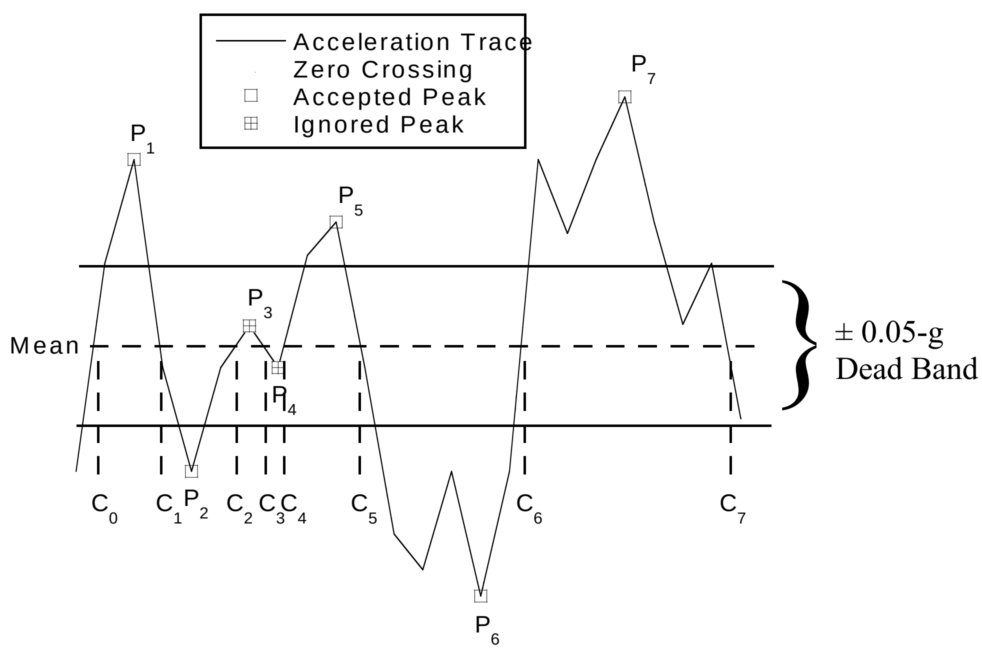

Figure 2. Peak-Between-Means Peak Counting Criteria

3.2 DATA PROCESSING PROCEDURES.

The time history file for vertical load factor records n_z. The data are then processed and presented in terms of Δn_z. The incremental vertical load factor, Δn_z, is equal to the vertical load factor, n_z, minus one. The incremental vertical load factors are due to maneuvers and gusts.

When the incremental vertical load factor data are processed for an OLMP report, a file is created for each flight that contains the sequential order of the peaks counted using the peak-between-means criteria. In addition to the peak magnitude and time data, information about the flight phases and coincident values, such as coincident airspeed, altitude, and gross weight, are stored. Table 2 shows a sample of the peaks file data from the cruise phase as counted by the peak-between-means algorithm along with other retained values, such as calibrated airspeed, time, and pressure altitude.

Table 2. Sample of the Counted Peaks File Data From the Cruise Phase

Peak	Time	Δn_z	Airspeed (knots)	Altitude (ft)
1	659.16	0.128	159	1061
2	662.41	-0.101	162	1106
3	663.66	0.068	163	1133
4	664.91	0.068	164	1193
5	665.53	0.059	167	1193
6	666.53	-0.06	167	1223
7	667.16	0.091	168	1249
8	669.66	0.077	169	1310
9	671.28	-0.124	170	1390
10	672.41	0.059	171	1430
11	672.78	-0.124	171	1430
12	674.16	0.059	170	1507
13	675.78	-0.142	170	1547
14	680.03	0.1	176	1742
15	681.16	-0.051	176	1781
16	683.41	-0.101	175	1867
17	684.53	0.119	176	1908
18	686.16	-0.101	174	1991
19	687.78	-0.083	175	2036
20	688.66	0.1	176	2072

The incremental vertical load factor (Δn_z) peaks are saved in 0.1 Δn_z increment bins as they are counted. This creates an incremental vertical load factor file for all counted occurrences in each increment of 0.1 Δn_z for the total number of flights (see columns 1, 2, 6, and 7 of table 3). All occurrences in each bin are assumed to be at the low end of that bin increment, as shown in columns 3 and 8 of table 3. The total cumulative occurrences (i.e., exceedances) that exceed the lowest $\pm\Delta n_z$ level is the sum of all ± occurrences and is given in the first row of columns 4 and 9 of table 3. The number of exceedances of any level is equal to the number of exceedances of the next lowest level less the number of occurrences at that level. Exceedances per 1000 hours (columns 5 and 10 of table 3) are determined by dividing the exceedances in columns 4 and 9 by 46554.6 hours and then multiplying by 1000 hours.

Table 3. Counted and Binned Peak Occurrences and Cumulative Occurrence for ERJ-145

1	2	3	4	5	6	7	8	9	10
$-\Delta n_z$ Bin Increment	Counted Occurrences per 46,554.6 Hours, 25,133 Flights	$-\Delta n_z$	Cumulative Occurrences per 46,554.6 Hours	Cumulative Occurrences per 1000 Hours	$+\Delta n_z$ Bin Increment	Counted Occurrences per 46,554.6 Hours, 25,133 Flights	$+\Delta n_z$	Cumulative Occurrences per 46,554.6 Hours	Cumulative Occurrences per 1000 Hours
-0.05 to -0.1	2881590	-0.05	3785494	81313	+ 0.05 to + 0.1	2997278	0.05	4172456	89625
-0.1 to -0.2	808258	-0.1	903904	19416	+ 0.1 to + 0.2	1011003	0.1	1175178	25243
-0.2 to -0.3	82013	-0.2	95646	2055	+ 0.2 to + 0.3	137521	0.2	164175	3527
-0.3 to -0.4	10752	-0.3	13633	293	+ 0.3 to + 0.4	21593	0.3	26654	573
-0.4 to -0.5	2067	-0.4	2881	62	+ 0.4 to + 0.5	3862	0.4	5061	109
-0.5 to -0.6	561	-0.5	814	17	+ 0.5 to + 0.6	834	0.5	1198	26
-0.6 to -0.7	152	-0.6	253	5	+ 0.6 to + 0.7	237	0.6	365	8
-0.7 to -0.8	53	-0.7	101	2	+ 0.7 to + 0.8	66	0.7	128	3
-0.8 to -0.9	29	-0.8	48	1	+ 0.8 to + 0.9	29	0.8	62	1
-0.9 to -1.0	10	-0.9	19	0	+ 0.9 to + 1.0	12	0.9	33	1
-1.0 to -1.1	3	-1	9	0	+ 1.0 to + 1.1	9	1	21	0
-1.1 to -1.2	3	-1.1	6	0	+ 1.1 to + 1.2	7	1.1	12	0
-1.2 to -1.3		-1.2			+ 1.2 to + 1.3		1.2		
-1.3 to -1.4	2.0	-1.3	3	0	+ 1.3 to + 1.4	2	1.3	5	0
-1.4 to -1.5		-1.4			+ 1.4 to + 1.5	1	1.4	3	0
-1.5 to -1.6		-1.5			+ 1.5 to + 1.6		1.5		
-1.6 to -1.7	1.0	-1.6	1	0	+ 1.6 to + 1.7		1.6		
-1. 7 to -1.8		-1.7			+ 1. 7 to + 1.8	1	1.7	2	0
-1.8 to -1.9					+ 1.8 to + 1.9	1	1.8	1	0
-1.9 to -2.0					+ 1.9 to + 2.0		1.9		

The data in columns 3, 5, 8, and 10 were used to plot the curves shown in figure 3. The exceedance curve is one of the common formats for incremental vertical load factor data presented in the FAA OLMP reports and is also used in this report to develop comprehensive sequences for the regional jet.

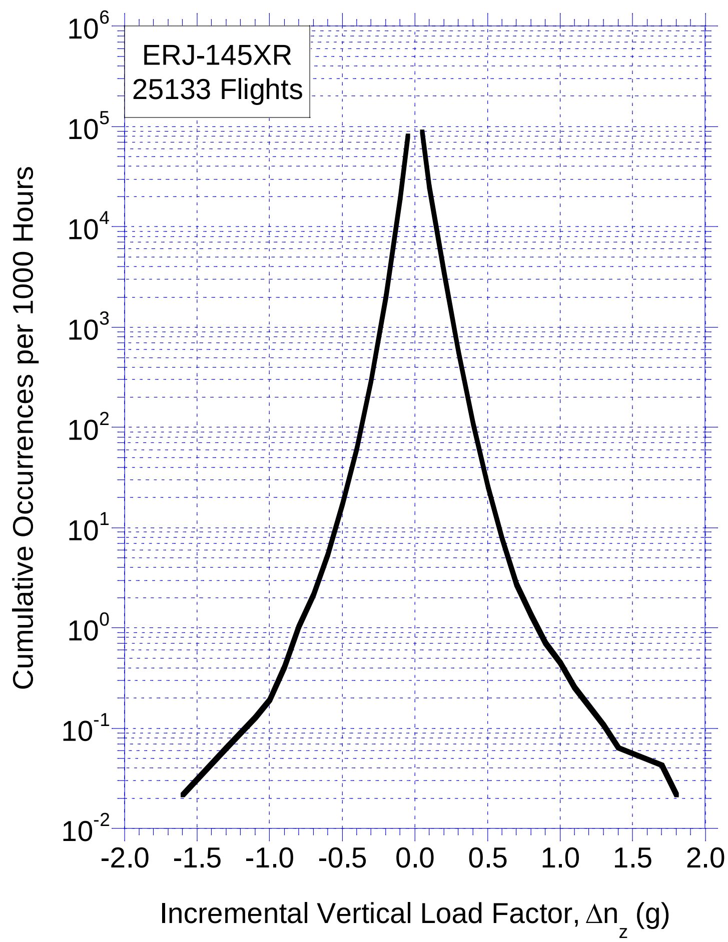

Figure 3. Incremental Vertical Load Factor Exceedances per 1000 hours (Combined Flight Phases, Manuever, and Gust) Data for ERJ-145

4. TASK 1: DEVELOPMENT OF COMPREHENSIVE STRESS SEQUENCES.

In task 1, comprehensive sequences of longitudinal skin stress at the fuselage crown above the wing were developed for a B-777, B-737, and ERJ-145. A number of simplifying assumptions were used to develop these sequences. T he resulting sequences are considered to be conservative approximations of actual sequences and capture the general characteristics of the three different sizes of large transport airplane.

The steps used to develop the comprehensive stress sequences are explained in the following sections.

4.1 MISSION PROFILES.

A single mission profile, as shown in figure 4, was used for each airplane model. It contains a preflight ground segment, one flight segment, a touchdown segment, and a postflight ground segment.

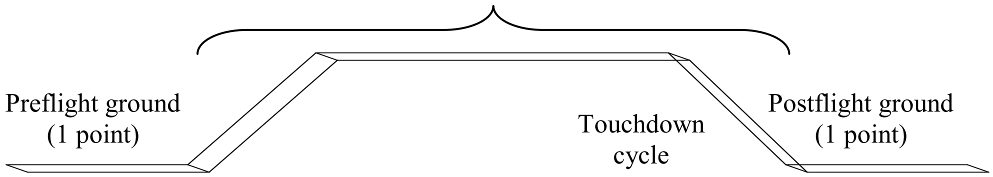

Figure 4. Single Mission Profile

The duration of the flight segment for each airplane model was determined from published usage data and is given in table 4 along with the number of flights recorded, average length, and average altitude for reference purposes.

Table 4. Flight Segment Duration

	Number of Flights	Average Flight Length (nm)	Average Duration (hours)	Average Maximum Altitude (ft)
ERJ-145	25,133	728.130	1.852	31,566
B-737-400	62,264	563.755	1.471	29,649
B-777-200	10,047	3035.992	6.669	37,392

The longitudinal skin stress was assumed to be constant and zero on the ground. The single-flight segment was assumed to be at maximum design altitude for each airplane model. This results in a steady-state skin stress due to maximum design cabin differential pressure (σ_{1P}). It was also assumed that the airplane configuration remained constant during the flight, which resulted in a steady-state inertia stress (σ_{1g}). Occurrences of incremental vertical load factors due to maneuvers and gusts during all phases of flight were considered, as discussed in sections 4.2 and 4.3.

4.2 FLIGHT SEGMENT INCREMENTAL VERTICAL LOAD FACTOR OCCURRENCES.

It is standard industry practice to develop sequences for analysis and tests that represent one tenth of an airplane's design life [2 and 4]. A design life of 60,000 flights was assumed for all three airplane models, therefore, sequences representing 6000 flights of usage were developed. To do this, the number and magnitude of incremental vertical load factors that could be expected in 6000 flights of usage had to be determined. This was accomplished using incremental vertical load factor exceedance data that were published for each model (e.g., figure 3 for the ERJ-145). The procedure was the same for each model and is described below for one $+\Delta n_Z$ level for the ERJ-145.

The procedure used to convert exceedances to occurances is shown in figure 5. The difference between the number of exceedances of $+\Delta n_Z = 0.6$ and the number of exceedances of $+\Delta n_Z = 0.7$ (both per 1000 hours) gives the number of occurrences of $+\Delta n_Z = 0.65$ per 1000 hours due to maneuvers and gusts for all flight phases, as shown below. This number is then used to determine the number of occurrences per 6000 flights using the hours per flight from table 4.

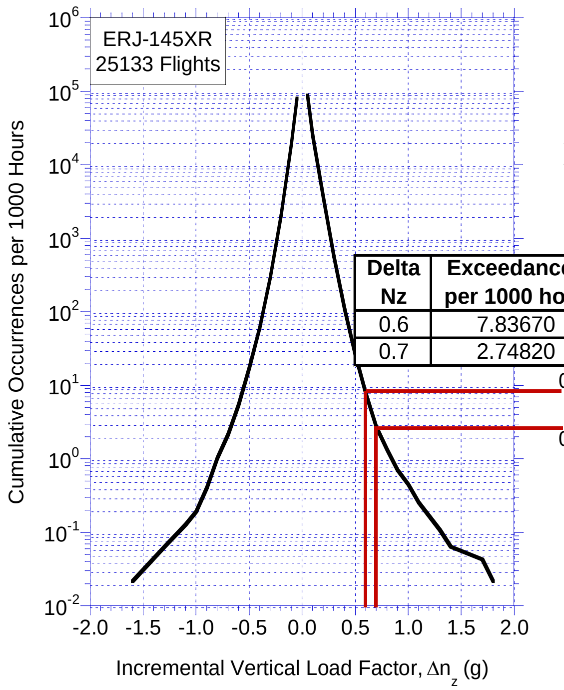

$$\text{Average Duration} = \frac{\text{Total Hours}}{\text{Total Flights}} = \frac{46{,}554.6}{25{,}133} = 1.8523$$

1 Flt = 1.8523 Hr

Delta Nz	Exceedances per 1000 hour	Occurrences per 1000 hour	Delta Nz	Occurrences per flight	Occurrences per 6000 flights
0.6	7.83670	5.08850	0.65	0.00943	56.59
0.7	2.74820				

Figure 5. Converting From Exceedances per 1000 Hours to Occurrences per 6000 Flights

This process was repeated for all positive and negative Δn_Z levels to determine the occurrences given in table 5. Another standard practice is to eliminate (or clip) levels that occur less than once per tenth of an airplane's design life. This is to eliminate unrepresentative crack growth retardation that can occur due to high, infrequent load levels. For this effort, levels occurring less than 0.5 times in 6000 flights were eliminated.

Table 5. The ERJ-145 Load Factor Flight Segment Tabular Spectra for 6000 Flights

$-\Delta n_z$ (g)	Occurrences	Cumulative Occurrences	$+\Delta n_z$ (g)	Occurrences	Cumulative Occurrences
-0.075	685,979	901,903	0.075	713,370	994,097
-0.15	193,077	215,924	0.15	241,509	280,727
-0.25	19,591	22,847	0.25	32,851	39,218
-0.35	2,569	3,256	0.35	5,158	6,367
-0.45	494	687	0.45	923	1,209
-0.55	134	193	0.55	199	286
-0.65	36	59	0.65	57	87
-0.75	13	23	0.75	16	30

Table 5. The ERJ-145 Load Factor Flight Segment Tabular Spectra for 6000 Flights (Continued)

$-\Delta n_z$ (g)	Occurrences	Cumulative Occurrences
-0.85	7	10
-0.95	2	3
-1.05	1	1
-1.15		
-1.25		

$+\Delta n_z$ (g)	Occurrences	Cumulative Occurrences
0.85	7	14
0.95	3	7
1.05	2	4
1.15	1	2
1.25	1	1

4.3 RANDOMIZED LOAD FACTOR SEQUENCE.

Because the load factor occurrences in table 5 no longer have a time history associated with them, they were considered to have occurred randomly. Thus, when forming a flight-by-flight, cycle-by-cycle load sequence from the statistical occurrence data, a procedure needed to be defined to ensure that the order of the cycles contained in the 6000-flight block was random. The paragraphs below describe how the occurrence spectra were randomized for the comprehensive sequence.

The technique used to distribute the load factors in a random fashion over 6000 flights are described using the flight segment spectra derived from the process shown in figure 5. Table 5 shows that the negative and positive occurrence spectra do not have the same number of cumulative occurrences. For the ERJ-145, the cumulative occurrence of the positive load factor peaks were greater than the negative spectrum.

To ensure that all 6000 flights in the block have the same number of cycles, it was necessary for the highest cumulative occurrence value (positive or negative) to be divisible by the size of the flight block. Since the cumulative occurrence value was not evenly divisible by 6000, cycles from lowest incremental load factor level (also the level with the greatest number of occurrences, 0.075 g) had to be truncated.

Using the values in table 5 as an example, the cumulative occurrences for the positive load factors divided by 6000, leaves a whole number remainder of 4097 occurrences that were truncated from the lowest Δn_z level of 0.075 g. The values are truncated from the lowest Δn_z level since, on their own, their contributions to damage were virtually nonexistent. The new cumulative occurrence total of 990,000 means that for the ERJ-145 flight segment, there were 165 cycles (990,000/6,000 = 165).

The approach used to pair the randomized positive and negative load factor occurrences assumed a symmetric number of cumulative occurrences. The recorded load factor data for the ERJ-145 shown in table 5 revealed that there were more occurrences of positive incremental vertical load factor than the negative vertical load factor. Occurrences of 0-g incremental (1-g) load factors were added to the negative occurrence spectrum to offset the difference between the cumulative totals of positive and negative occurrences. A half cycle is a cycle that combines a 1-g load factor with a positive load factor occurrence. The number of 0-g Δn_z or 1-g n_z occurrences added to the negative occurrence spectrum was equal to the difference between the truncated positive and negative spectra (990,000 - 901,903 = 88,097). Because each flight begins with a ground load paired with a random flight stress, there needs to be 6000 fewer negative flight occurrences (one per flight) to maintain an even number of positive and negative occurrences to form random pairs/cycles. Therefore, instead of 88,097 occurrences of zero incremental load factors being added, the actual number was 88,097 - 6,000 = 82,097.

Figure 6 shows incremental vertical load factor exceedances per 6000 flights for the three airplane models considered. Note that the smaller ERJ-145 has a more severe load factor spectrum than the B-737 and B-777 airplane.

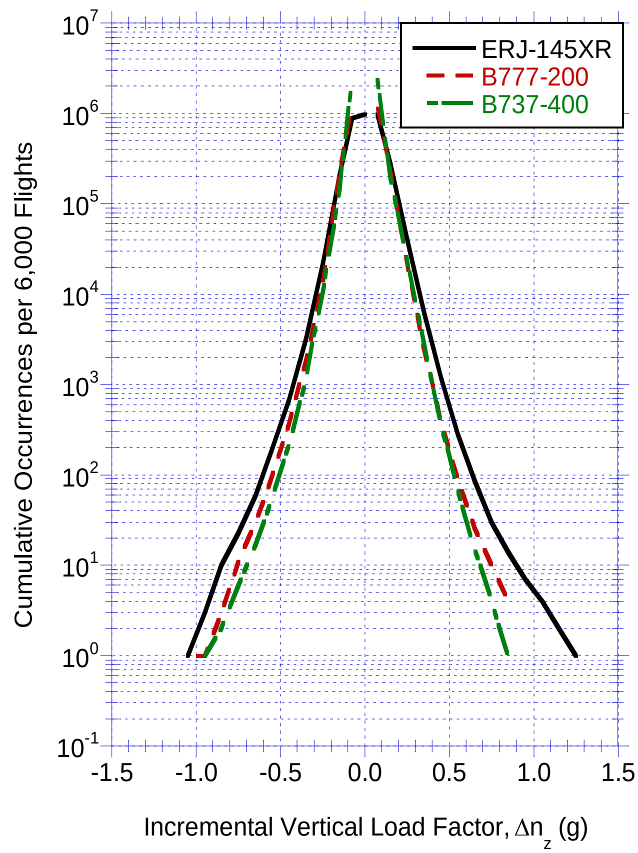

Figure 6. Incremental Vertical Load Factor Exceedances per 6000 Flights for the Three Considered Airplane Models

The positive and negative Δn_Z occurrences that were determined for each airplane model are listed in table 6. These were used to randomly populate each flight in each 6000-flight comprehensive sequence. Note that, unlike the ERJ-145 recorded vertical load factor data, the B-737 and B-777 occurrence spectra had more negative than positive occurrences. As a result, occurrences of 0-g incremental vertical load factor were added to the positive occurrence spectrum for these two airplanes to be able to form the half cycles required for symmetric spectra.

Table 6. Incremental Vertical Load Factor Occurrences for the Three Considered Airplane Models

ERJ-145			
(-)Δn_z	Occurrences	Occurrences	(+)Δn_z
0	82,097	709,273	0.075
-0.075	685,979	241,509	0.15
-0.15	193,077	32,851	0.25
-0.25	19,591	5,158	0.35
-0.35	2,569	923	0.45
-0.45	494	199	0.55
-0.55	134	57	0.65
-0.65	36	16	0.75
-0.75	13	7	0.85
-0.85	7	3	0.95
-0.95	2	2	1.05
-1.05	1	1	1.15
		1	1.25
B-737-400			
(-)Δn_z	Occurrences	Occurrences	(+)Δn_z
-0.075	2,323,459	9,215	0
-0.15	137,427	2,273,303	0.075
-0.25	9,936	173,253	0.15
-0.35	961	19,388	0.25
-0.45	162	2,477	0.35
-0.55	38	295	0.45
-0.65	11	54	0.55
-0.75	4	11	0.65
-0.85	1	3	0.75
-0.95	1	1	0.85

Table 6. Incremental Vertical Load Factor Occurrences for the Three Considered Airplane Models (Continued)

B-777-200			
(-)Δn_z	Occurrences	Occurrences	(+)Δn_z
-0.075	1,048,924	77,842	0
-0.15	208,673	971,570	0.075
-0.25	12,561	207,063	0.15
-0.35	1,467	19,033	0.25
-0.45	278	2,100	0.35
-0.55	67	298	0.45
-0.65	19	68	0.55
-0.75	8	16	0.65
-0.85	2	6	0.75
-0.95	0	4	0.85
-1.05	1		

Each flight in each 6000-flight block is populated by using a random-number generator to select and pair negative and positive load factor occurrences. The method used to pair the occurrences is a full-cycle unrestrained method, which means that a random negative incremental load factor value is paired with a random positive incremental load factor value. The appropriate number of cycles were formed by randomly extracting negative and positive incremental load factors from the occurrences given in table 6. When the process was complete, a unique block of 6000 random flights was created for each airplane type. Figure 7 shows a randomized incremental vertical load factor sequence within the flight segment of one ERJ-145 flight.

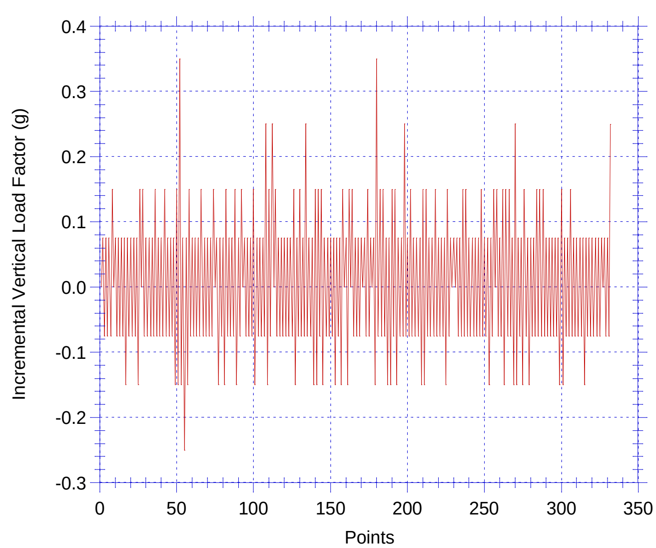

Figure 7. Comprehensive Incremental Load Factor Sequence for the Flight Segment of One ERJ-145 Flight

The touchdown event consisted of a single cycle. The touchdown occurrences per 6000 flights were derived in a similar fashion to the flight segment that was discussed in the previous paragraph.

The incremental load factor sequences were used to generate longitudinal skin stress sequences, as described in the following sections.

4.4 GENERATION OF LONGITUDINAL SKIN STRESS SEQUENCES.

The longitudinal stress in the fuselage skin at the crown above the front spar is due to cabin pressurization and inertia and is given by

$$\sigma_L = \sigma_{1P} + \sigma_{1g}(1 + \Delta n_z) \tag{1}$$

where

σ_L = total longitudinal stress
σ_{1P} = longitudinal stress due to cabin pressurization
σ_{1g} = longitudinal stress due to steady state inertia at 1 g
Δn_z = incremental vertical load factor

For sequence generation purposes, it is assumed that σ_L is constant and zero is on the ground.

Equation 1 is used to transform the incremental vertical load factor sequences for the flight segments of each of the 6000 f lights in the repeatable blocks for each of the models to longitudinal stress sequences. Calculation of the pressure and inertia components of skin stress is discussed below.

4.4.1 Pressure Stress.

The pressure component of the longitudinal skin stress was calculated using the equation for the longitudinal membrane stress in a thin-walled, cyclindrical pressure vessel given below.

$$\sigma_{1P} = \Delta P r/2t \tag{2}$$

where

ΔP = maximum design cabin differential pressure
r = fuselage radius
t = skin thickness

Use of equation 2 results in a co nservative value of stress since the beneficial effect of the longerons is neglected (i.e., this assumes the skin reacts all the pressure loading). The ΔP, r, and t used for each airplane model and the resulting σ_{1P} is given in table 7.

Table 7. Comparison of Stress Calculation Variables and Calculated Stress Levels for ERJ-145, B-737, and B-777 Airplanes

Airplane	r (in.)	ΔP (psi)	t (in.)	σ_{1P} (psi)	σ_{1g} (psi)	σ_L at 1 g (psi)
ERJ-145	45	7.8	0.05	3,510	13,182	16,692
B-737	74	7.8	0.036	8,017	11,125	19,142
B-777	122	8.6	0.071	7,389	11,450	18,839

4.4.2 Inertia Stress.

The 1-g inertia component of the longitudinal skin stress at the crown of the fuselage can be reasonably estimated by assuming that the limit design condition that sizes this area is a 2.5-g symmetric maneuver combined with maximum design cabin differential pressure plus 1.1 psi. Additionally, it is assumed that there is a zero margin of safety for the skin (2024-T3 material for all three models) at ultimate load. Consistent with these assumptions the longitudinal stress due to steady state inertial loading at 1 g is given by

$$\sigma_{1g} = \frac{C_{kd}\left(\frac{F_{tu}}{1.5}\right) - \frac{(\Delta P + 1.1)r}{2t}}{2.5} \tag{3}$$

where

C_{kd} = knockdown factor applied to account for the assembled structure and is equal to 0.88 based on experimental data

F_{tu} = ultimate tensile strength (63,000 psi for 2024-T3 sheet [5])

ΔP = is the maximum design cabin pressure differential

r = is the fuselage radius

t = skin thickness

The ΔP, r, and t used for each airplane model and the resulting σ_{1g} is given in table 7.

Figure 8 shows a comprehensive stress sequence for one ERJ-145 flight that was generated using equation 1 and an ERJ-145 incremental vertical load factor sequence.

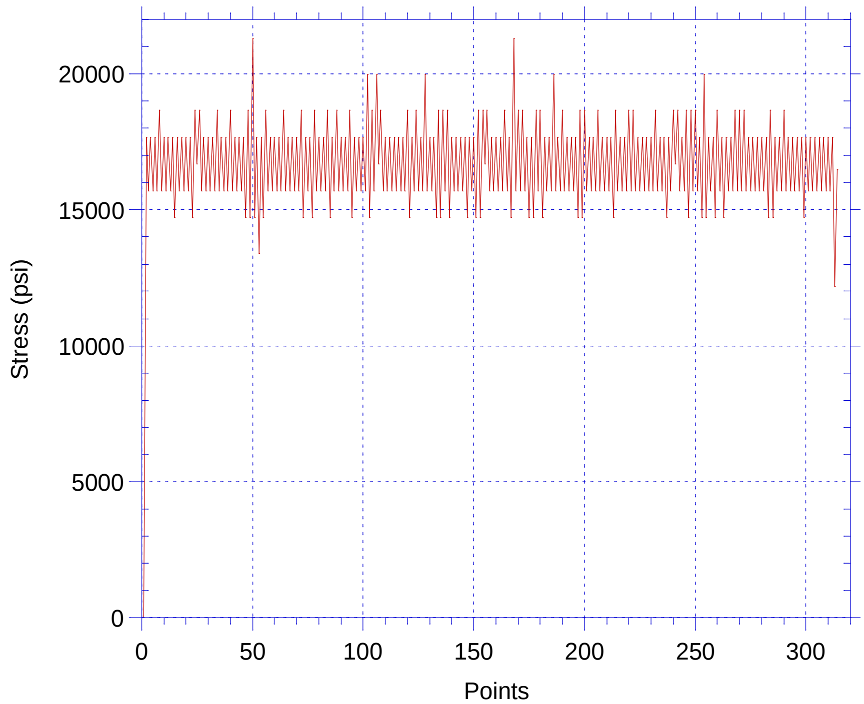

Figure 8. An ERJ-145 Comprehensive Stress Sequence, One Flight

4.5 STRESS SEQUENCE TRUNCATION.

A low level of truncation was applied to the comprehensive stress sequence prior to running the coupon test. Stress sequences are often truncated prior to testing to remove nondamaging cycles. Reducing the number of endpoints within the sequence reduces the amount of time required to run the fatigue tests. Cycles with a delta stress less than 1000 psi were removed from the sequence leaving the remaining random order of the comprehensive sequence intact. This minimal delta stress level affects only cycles that contain the lowest possible stress cycle generated when a 0-g Δn_z point is paired with a ±0.075-g Δn_z point. Table 8 shows the magnitude of the truncated delta stress cycle and the reduction in the number of cycles in the resulting 6000-flight block for each considered models.

Table 8. Truncated Stress Levels and Truncation Results

Airplane	Delta Stress (psi)	Occurrences per Flight Block	Total Cycles per Block	Cycles per Block After Truncation	Percent of Cycles Truncated
ERJ-145	989	59,120	996,000	936,880	5.936
B-737	834	8,671	2,484,000	2,475,329	0.349
B-777	859	63,765	1,284,000	1,220,235	4.966

5. TASK 2: DEVELOPMENT OF CONSTANT-AMPLITUDE STRESS SEQUENCES.

The primary objective of this task, as discussed in section 1 and shown in figure 1, is to determine what n_{ZE} should be for a constant-amplitude sequence defined by

$$\sigma_{max} = \sigma_{1P} + n_{ZE}\sigma_{1g} \quad R = 0 \tag{4}$$

to result in equal or conservative-bounding crack growth when compared to the results of a corresponding comprehensive sequence.

Constant-amplitude sequences were developed for each of the airplane models using the same values of σ_{1P} and σ_{1g} that were used to generate corresponding comprehensive sequences (see table 7). Three sequences were developed for the B-777 using n_{ZE} = 1.1, 1.15, and 1.3. One sequence was generated for the B-737 and one for the ERJ-145 using n_{ZE} = 1.3.

6. TASK 3: CRACK GROWTH TESTS.

Under task 3, all the sequences developed under tasks 1 and 2 were applied to small test coupons, and crack growth data was generated and compared. Test program details are included in appendix A and information on data editing that was performed is included in appendix B. A summary of this information is included in sections 6.1 through 6.5.

6.1 TEST COUPON CONFIGURATION.

The test coupon configuration shown in figure 9 was used for all tests. The only difference was thickness, which is noted. The coupon material was a 2024-T3 aluminum sheet that was fabricated to meet the specifications of ASTM E 647-99 for a middle-tension coupon. Overall dimensions are given in figure 9. A center through slot, approximately 0.375″ long, was introduced using electrical discharge machining (EDM) as shown.

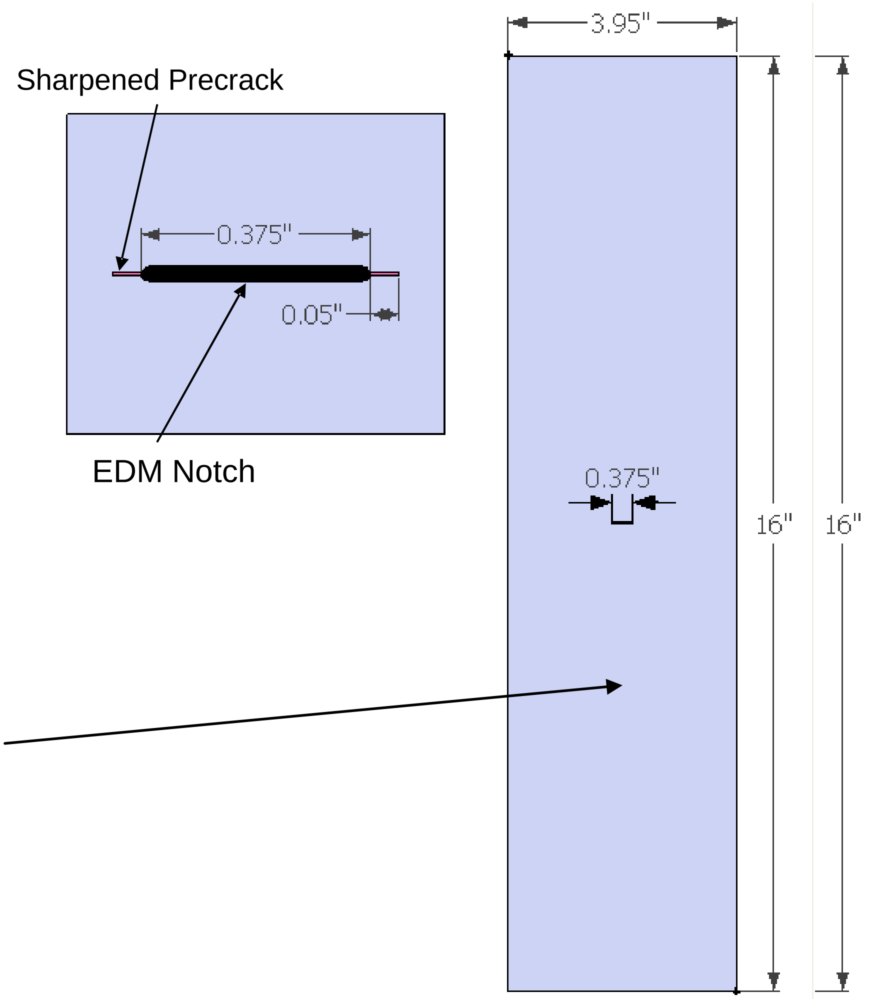

Model	*t* (in.)
ERJ-145	0.04
B-737	0.04
B-777	0.071

Figure 9. Test Coupon Configuration

6.2 TEST COUPON LOADING.

The comprehensive and constant-amplitude stress sequences were transformed into load sequences by multiplying by the gross area of the coupon. A dditionally, the previously discussed assumption that the longitudinal skin stress is zero on the ground had to be modified because achieving a zero test loading condition can be problematic. Therefore, the zero stress/load state on the ground was replaced with a near zero load. The resulting maximum stress and corresponding load and ground stress and corresponding load for each sequence is given in table 9.

Table 9. Test Matrix Ranges of Stress and Load

Airplane	Tests	Maximum Stress	Ground Stress	Maximum Load	Ground Load
		psi		lb	
ERJ-145	Comprehensive	33,170	206	5,241	32.5
	CA 1.3	20,647	206	3,262	32.5
B-737	Comprehensive	28,598	206	4,518	32.5
	CA 1.3	22,480	206	3,552	32.5
B-777	Comprehensive	28,572	160	8,013	45
	CA 1.3	22,274	160	6,247	45
	CA 1.15	20,556.5	160	5,765	45
	CA 1.1	19,984	160	5,605	45

CA = Constant-amplitude sequence

6.3 TEST PROCEDURE.

Prior to applying the sequences and collecting data, each coupon was subjected to precrack loading to initiate and grow a fatigue crack out of each end of the EDM slot, as indicated in figure 9. A load-shedding technique was used to achieve an average crack extension of 0.05″ from both ends of the center EDM slot.

After precracking, the sequences were applied. Three tests were performed for each comprehensive and constant-amplitude sequence. A traveling microscope with a resolution of 1×10^{-5} meters was used to measure crack extension from both ends of the EDM slot. The average crack extension was added to the EDM slot half length (i.e., 0.375″/2) to determine the half crack size. The half-crack size versus number of flights data for each coupon tested is included in appendix A. The average of the three tests for each sequence is also shown in the half-crack size versus flights plots.

6.4 da/d_{Flight} AND DATA EDITING.

When the comprehensive sequence data was obtained for some tests during the early stages of growth, it was noted that the growth rate decreased instead of increasing, as would be expected. To further investigate this apparent anomaly, the crack growth rate per flight (da/d_{Flight}) was calculated as a function of crack length. These data are presented in appendix B. The largest initial decrease occurred for the ERJ-145 sequence on test number 1 (see figure B-1). The trend was not always present, and when it was, the magnitude varied significantly. However, it was noted that by the time the half-crack length was about 0.375″, the nominal rate was increasing in a relatively stable manner for all tests conducted. The cause of the initial decrease was not investigated any further. For the purpose of this effort, it was decided to discard all crack growth data prior to a half-crack length of 0.375″ for all sequences before comparing the results.

6.5 RESULTS.

The crack growth results from the comprehensive and constant-amplitude sequences are shown in figures 10 through 12 for the ERJ-145, B-737, and B-777, respectively. Each curve is the average of three tests. The crack growth resulting from the constant-amplitude sequences using n_{ZE} = 1.3 conservatively bounds the crack growth that resulted from the comparable comprehensive sequences for all three large transport airplane models considered.

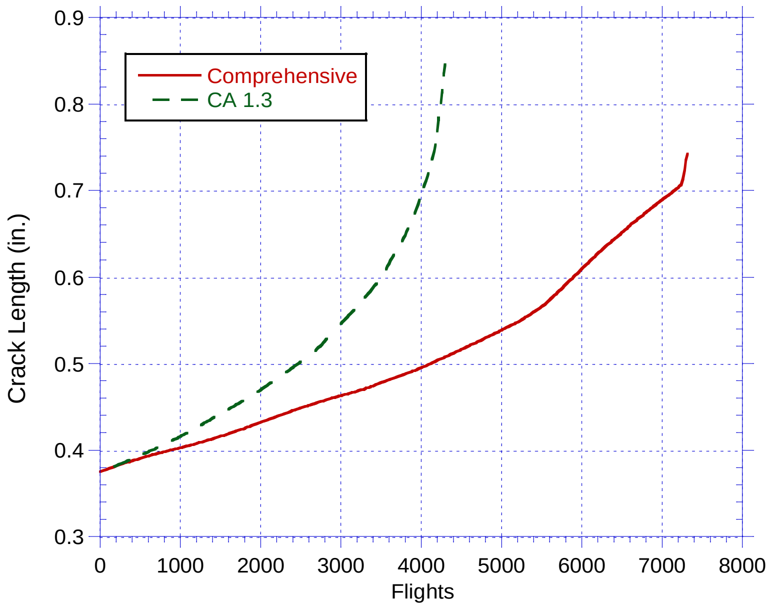

Figure 10. The ERJ-145 Crack Growth Results

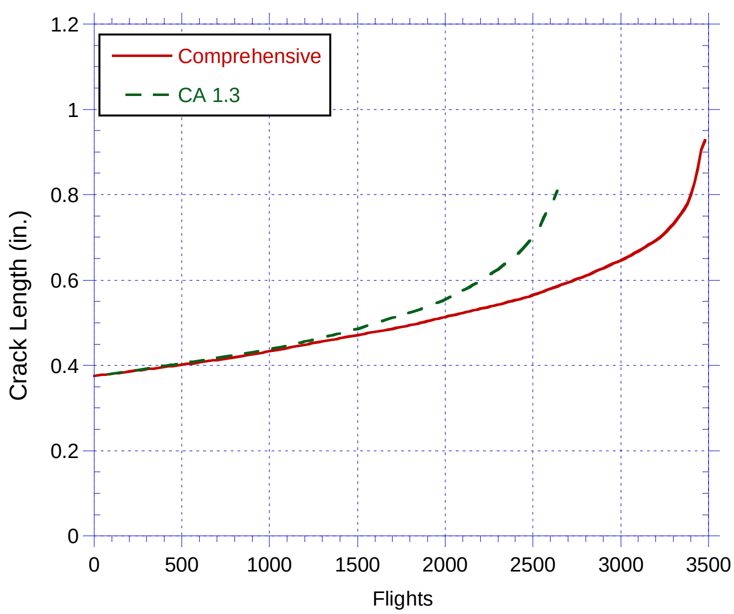

Figure 11. The B-737 Crack Growth Results

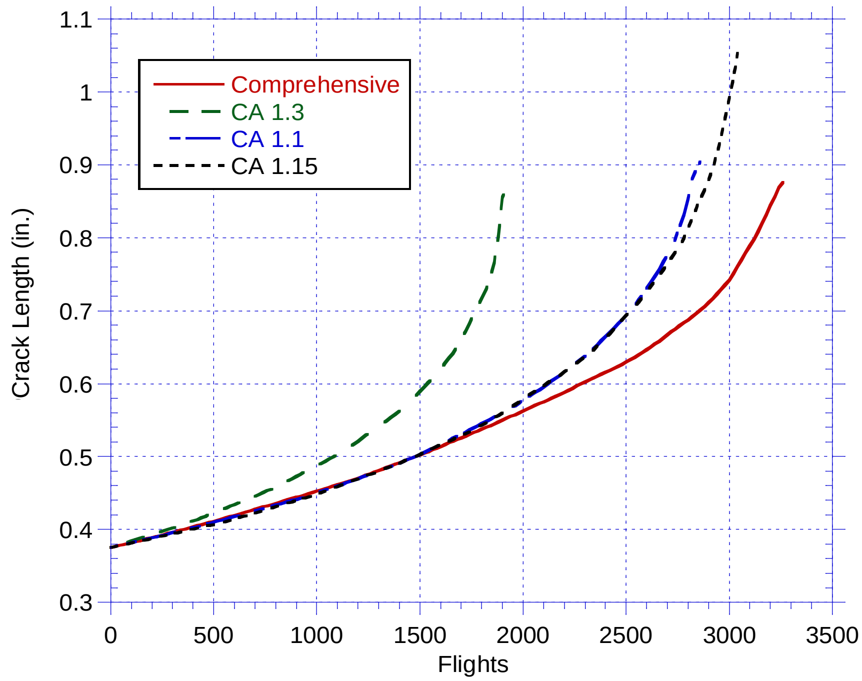

Figure 12. The B-777 Crack Growth Results

7. CONCLUSIONS.

Based on the work performed under this effort it is concluded that

- it is feasible to use a constant-amplitude stress sequence instead of a comprehensive stress sequence when assessing crack growth in fuselage pressure boundary structure.
- a conservative estimate of crack growth can be obtained provided the constant-amplitude stress sequence used consists of one cycle per flight with a stress ratio of zero and a peak stress due to cabin pressurization plus 1.3 times the stress due to steady state inertia.
- conclusions 1 and 2 are generally applicable to the fuselage pressure boundary structure of large transport airplanes.

8. REFERENCES.

1. De Jonge, J.B., "Reduction of Incremental Load Factor Acceleration Data to Gust Statistics," FAA report DOT/FAA/CT-94/57, August 1994.

2. Crabill, N., "FAA/NASA Prototype Flight Loads Program System Requirements: Boeing 737-400," Eagle Engineering, Inc., Contract NAS1-19659. ASC 92-045, November 7, 1995.

3. de Jonge, J.B., et al., “A Standardized Load Sequence for Flight Simulation Tests on Transport Aircraft Wing Structures” National Aerospace Laboratory, NLR TR 73029 C, March 1973.

4. Liu, A.F., “Mechanics and Mechanisms of Fracture: An Introduction,” ASM International, August 2005, pp. 382.

5. MIL-HDBK-5H “Metallic Materials and Elements for Aerospace Vehicle Structures,” U.S. Department of Defense, December 1998.

APPENDIX A—TEST MACHINE SETUP, TEST COUPON GEOMETRY, TEST PROCEDURE, AND RESULTS

1. INTRODUCTION.

Task 3 of the fuselage, simplified stress sequences for fuselage structure project required crack growth data to be collected from a series of coupon tests to allow for comparisons between the comprehensive stress sequences and the constant-amplitude sequences. This appendix outlines the test equipment and procedures used to complete the coupon test program. A brief description of the test coupon is also included. The equipment and procedures described below were used for each test to obtain consistent results.

The sequences that were tested and how they were developed is discussed in the main report.

2. TEST MACHINE DESCRIPTION.

A 20-kip, servo-hydraulic universal MTS® test machine was selected to run the tests for this research. The highest load applied during the tests was 8013 lb (B-777 comprehensive sequence), but for most of the tests (all ERJ-145 and B-737 tests), the load range was less than 4000 lb. The hydraulic grips on the MTS test machine could hold coupons up to 4 inches wide but required shim inserts to hold the thin sheet coupons in place.

As part of the experimental setup, studies were conducted through data acquisition and strain gage tests to verify the capability of the 20-kip load cell to accurately match the commanded loads during the tests. Initially, a data acquisition computer was set up to independently collect the command signal (signal from computer to controller) and the load cell response. Data was collected at a rate of 2.5 kilohertz. Data was collected from a representative segment of the ERJ-145 untruncated comprehensive sequence run at constant load rates of 14- and 10-kips-per-second. Comprehensive sequence tests were run using the control software's spectral sequence setup, which feeds the commanded points directly to the controller with no additional feedback loop. The maximum load in the sequence, which is used to check the accuracy of the test machine, was 2690 lb and the lowest load was equal to the 50-lb ground load.

Figure A-1 shows a time history trace of the stress values collected from the data acquisition computer. The figure also shows a table comparing the commanded load (exact delta stress for each cycle) to the load cell output delta stress that was applied to the test coupon. The highest error was approximately 3%, and the average error for the selected sequence was only -0.447%. The result below is for the 10-kip-per-second case. The 14-kip-per-second tests had slightly higher errors, but the results were less than 1% on average.

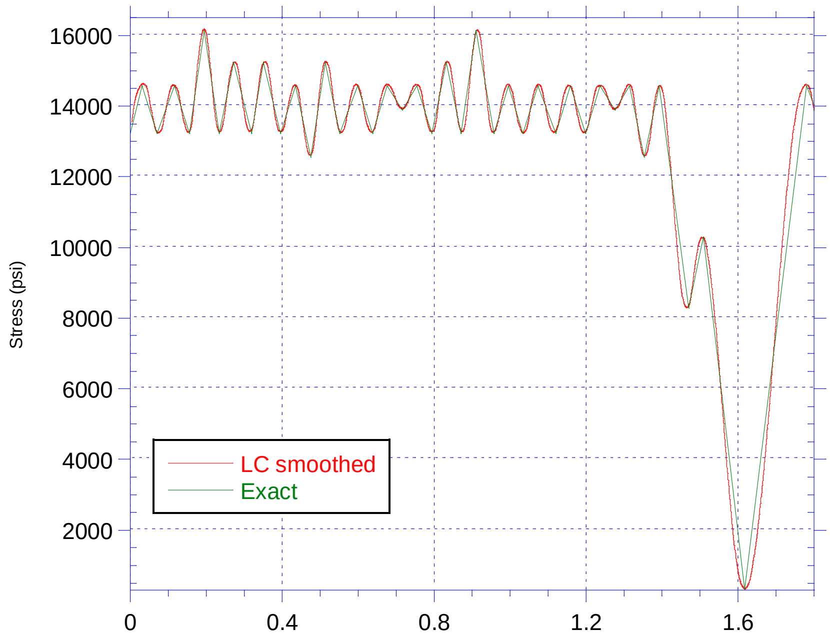

Exact delta (psi)	Load Cell Smoothed delta (psi)	% Error
1341.9	1349	0.529
2909.7	2907	-0.093
2013.8	1977	-1.827
2013.8	1966	-2.374
1341.9	1302	-2.973
2682.7	2661	-0.809
1341.9	1360	1.349
1341.9	1345	0.231
669.93	673	0.458
2013.8	1988	-1.281
2909.7	2870	-1.364
1341.9	1360	1.349
1341.9	1383	3.063
1341.9	1319	-1.707
1341.9	1318	-1.781
669.93	683	1.951
2010.8	2002	-0.438
2011.1	1954	-2.839
14252	14261	0.063
	Average Error (%)	-0.447

Figure A-1. Digital Acquisition Trace and Point-to-Point Comparison of Commanded Load and Load Cell Response

In addition to the data collected from the 20-kip load cell, a 5-kip load cell, which provided slightly improved capabilities in terms of matching the load sequence (20-kip load cell—average error -0.447% and 5-kip load cell—average error -0.178%), was used for several tests. Figure A-2 shows that the crack growth results from the 5-kip load cell were essentially identical to the tests performed using the 20-kip load cell.

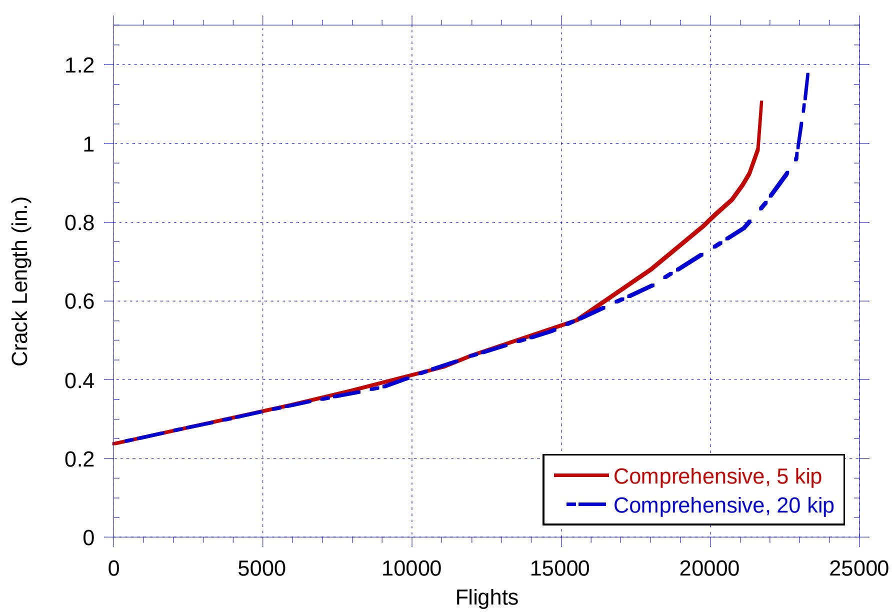

Figure A-2. Crack Growth Life of Sample Comprehensive Sequence Using 5- and 20-kip Load Cell

Since the loads for the B-777 airplane were outside the range of the 5-kip load cell, the decision was made to use the 20-kip load for all tests. The 20-kip load cell proved it was capable of reliably applying the correct loads to the test coupon and eliminated the need to exchange load cells on the test frame.

3. CONTROLLER SOFTWARE.

The Material Analysis and Testing Environment (MATE) software developed by the University of Dayton Research Institute (UDRI) provided the interface used to command the load cell. The MATE software allowed the load levels and tests rates for the precracking and constant-amplitude coupon tests to be easily controlled. The MATE software requires the comprehensive sequence be input as a single column. The values of the comprehensive sequence input file represent a fraction of the maximum load, and there must be at least one occurrence of the 1.0 value (maximum load) in the file. The comprehensive sequence input runs as a point-to-point loads sequence to model the operational usage as closely as possible. The comprehensive sequence is run open loop, and there is no feedback control loop.

The precracking and constant-amplitude tests were run using a high-frequency cycle capability within the MATE software that allowed for the controller to send a feedback loop to the servo valve in an attempt to optimize the load applied to the coupon. This high-frequency software feature within MATE runs a constant cycle that contains user-defined minimum and maximum load values and frequencies. The feedback loop is able help control the load cell to more accurately reach the fixed-load values.

4. TEST COUPONS.

The bare-aluminum 2024-T3 sheet chosen for this test effort is a common aluminum alloy used in fuselage applications. A single sheet of Al 2024-T3 in a nominal fuselage skin thickness of 0.04 inch was used for the ERJ-145 and B-737 test coupons and a sheet of 0.071″ thick Al 2024-T3 was used to machine the B-777 coupons. It should be noted that the 0.04″ and 0.071″ test coupons used came from a single sheet of the respective material thicknesses.

All machining, except for the electrical discharge machining (EDM) notch, was performed onsite in the UDRI machine shop. A diagram with the dimensions of the test coupon is shown in figure A-3. The 16″ length was necessary to meet requirements in ASTM E 647-99. When the coupon was placed into the load cell, the top and bottom 4″ were covered by the hydraulic grips, leaving only approximately 8″ of the coupon exposed.

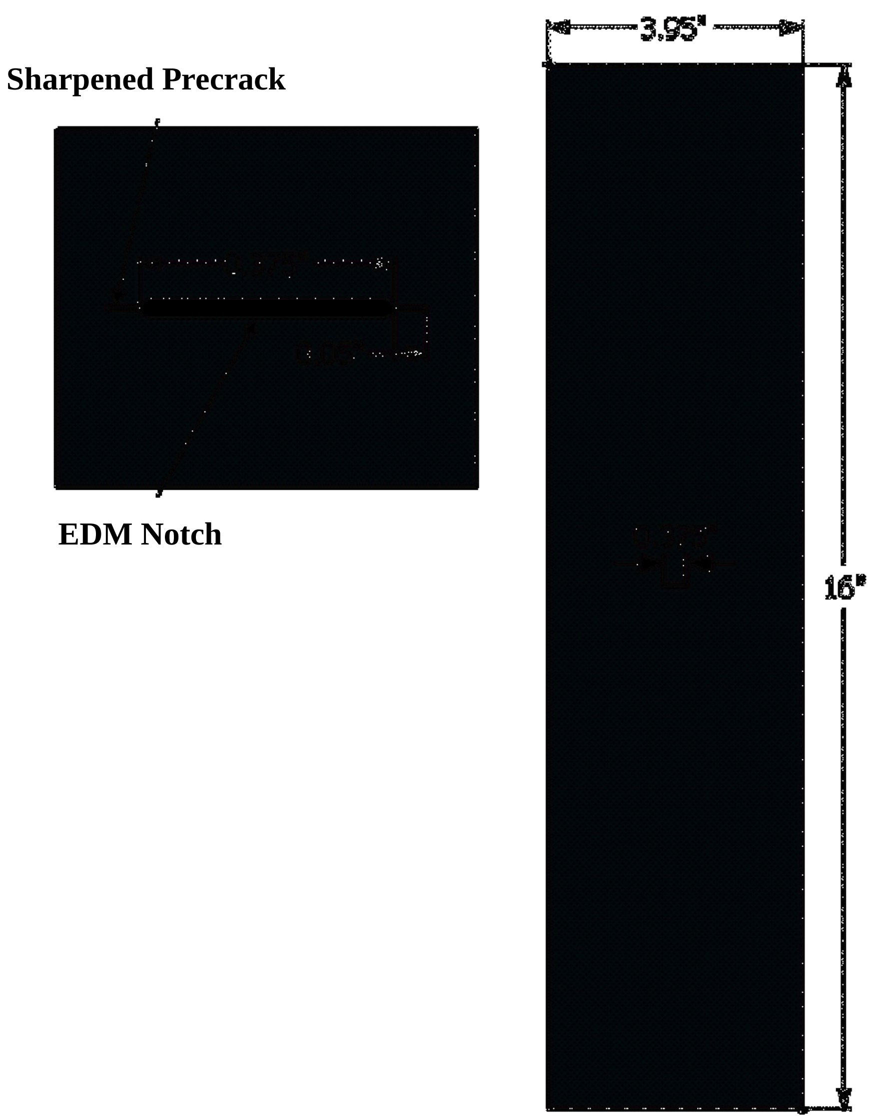

Figure A-3. Test Coupon Design

A Dremel® rotary tool with a 1/2″ felt polishing wheel attachment and a polishing compound was used to polish the tarnished area where the crack was predicted to grow. This step was performed to aid in the visual measurement of the crack tip during the coupon testing. The polished surface enhanced the reflected light from crack tip allowing for easier viewing. The time required to polish the coupon was minimal (about 5 minutes per coupon).

5. PRECRACKING.

The crack growth tests performed were middle-tension tests. Prior to any loads being applied to the test coupon, it underwent a precracking process. Each test coupon was precracked using a load-shedding technique to an initial average crack extension (left crack length and right crack length divided by two) of 0.05″ from the EDM notch. Information about load shedding is found in ASTM E 647-99. The precracking procedure takes about 1 hour to complete (around 30,000 cycles), and the final stress was about 1000 lb less than the mean stress in the comprehensive sequence. The initial maximum load applied for the 0.04″ coupon was 1800 lb and for the 0.071″ Al 2024-T3 the maximum load was 3500 lb. The cycles used for precracking had an R value of 0.1.

The object of the precracking procedure was to generate a sharp crack tip that would serve as a common starting point for all the tests.

6. PERFORMING TESTS.

There were two distinct types of tests run for this research, an open-loop variable load sequence and a high-frequency, constant-amplitude test. It was important for each type of tests run that every effort be made to ensure that the loads applied to the test coupon match the commanded load values as close as possible.

Comprehensive tests were run using a constant load rate of 15 kips per second. This range provided accurate reproduction of the commanded comprehensive load values. Therefore, a 6000-flight block run from start to finish would take over 24 hours.

The simplified constant-amplitude tests were run at a fixed frequency of 4 hertz. The constant-amplitude test required constant monitoring and could be run from start to finish in a few hours.

7. CRACK GROWTH MEASUREMENTS.

An optical traveling microscope was used to track and record the crack progress during testing. An automated crack growth detection method was not required due to the relatively low number of coupons tested. The traveling microscope had a resolution of 1×10^{-5} m.

The tabular data from each test run for each airplane type is shown in tables A-1 through A-8. It should be noted that since the final results were based on the average of three tests, it was not always necessary to run each test to failure. The average results of the three tests for a particular constant-amplitude (CA) level or comprehensive sequence was only calculated to the earliest failure. There was not an unreasonable amount of scatter in any of these test sequences; but conceivably, if the first run of a sequence failed earliest, then the next two tests would only have to be run to the number of flights where the first test failed. Included beneath each table is a plot of the individual tests with the averaged crack growth curve (figures A-4 through A-11).

Table A-1. The ERJ-145XR Comprehensive Test Results

Test 1		Test 2		Test 3	
Flights	Crack Length (in.)	Flights	Crack Length (in.)	Flights	Crack Length (in.)
0	0.238	0	0.238	0	0.238
571.87	0.257	869.6	0.262	1921.3	0.289
1121.3	0.279	1376.9	0.279	3842.5	0.326
1921.3	0.3	2727.8	0.298	6000	0.38
2881.9	0.309	3754	0.322	6960.6	0.403
4162.8	0.347	5123.4	0.352	8209.5	0.447
5123.4	0.366	6000	0.386	9061.3	0.464
6000	0.399	7120.7	0.411	10163	0.51
7143.6	0.426	8209.5	0.446	11027	0.551
8209.5	0.464	9106.1	0.476	11877	0.628
9384.4	0.492	9842.5	0.504	12000	0.64
10963	0.579	10479	0.522	12432	0.663
11568	0.631	11219	0.548	13057	0.708
11816	0.662	11849	0.606	13068	0.782
12000	0.687	12000	0.618		
12285	0.711	12389	0.64		
12564	0.73	12977	0.68		
12897	0.776	13162	0.729		
13025	0.824	13601	0.764		
13064	1.099	14049	0.797		
		14627	0.839		
		14952	0.867		
		15223	0.938		
		15298	1.035		

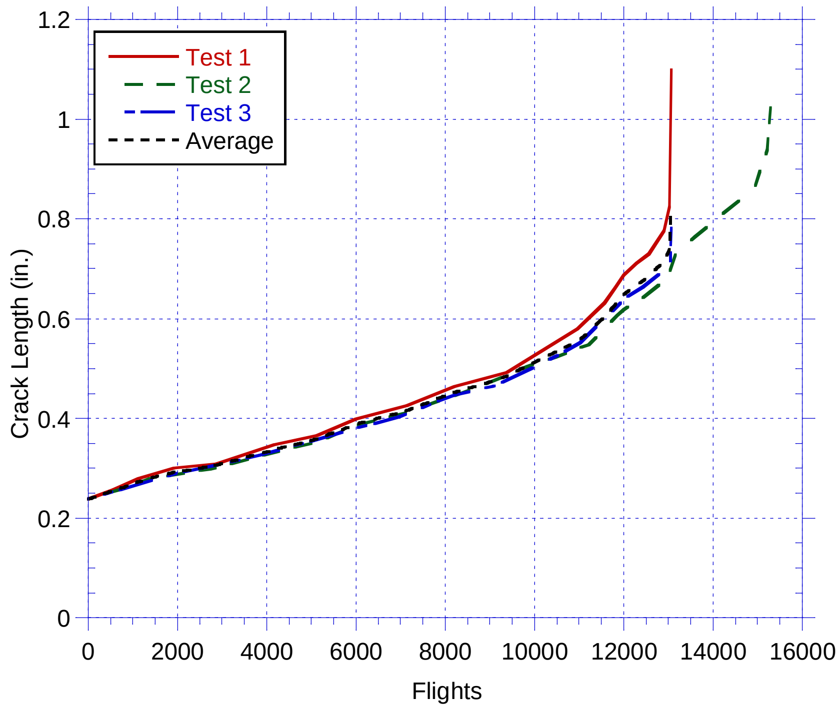

Figure A-4. The ERJ-145 Comprehensive Test Results and Average Curve

Table A-2. The ERJ-145 CA 1.3 Test Results

Test 1		Test 2		Test 3	
Flights	Crack Length (in.)	Flights	Crack Length (in.)	Flights	Crack Length (in.)
0	0.238	0	0.238	0	0.238
700	0.251	701	0.249	699	0.253
1500	0.272	1500	0.263	1502	0.269
2400	0.287	2400	0.279	2401	0.289
3400	0.313	3400	0.299	3400	0.314
4400	0.335	4401	0.321	4400	0.347
5400	0.366	5401	0.347	5400	0.381
6300	0.396	6301	0.378	6300	0.426
7300	0.443	7199	0.411	7200	0.478
8300	0.498	8001	0.454	8000	0.544
9179	0.574	8801	0.499	8700	0.636
9601	0.632	9501	0.559	9100	0.729
9903	0.7	10000	0.618	9325	0.821
10150	0.78	10450	0.703	9414	0.89
10315	0.9	10698	0.785		

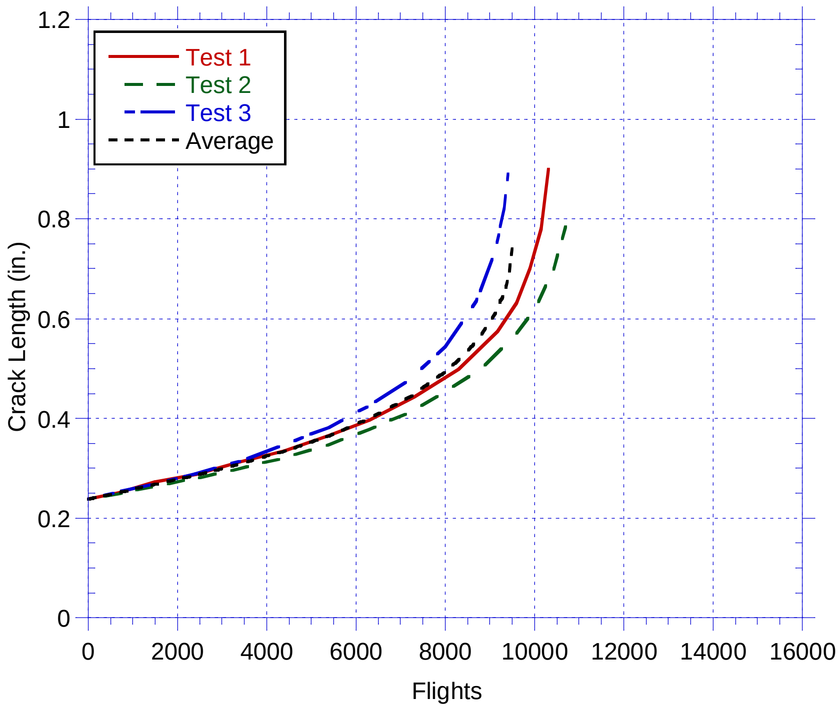

Figure A-5. The ERJ-145 CA 1.3 Test Results and Average Curve

Table A-3. The B-737 Comprehensive Test Results

Test 1		Test 2		Test 3	
Flights	Crack Length (in.)	Flights	Crack Length (in.)	Flights	Crack Length (in.)
0	0.238	0	0.238	0	0.238
156	0.245	359	0.253	361	0.253
570	0.259	1333	0.28	1390	0.28
1091	0.271	1718	0.294	1851	0.298
2149	0.317	2606	0.327	2993	0.348
2686	0.333	3636	0.372	4302	0.416
3575	0.376	4569	0.418	5211	0.486
4120	0.407	5124	0.46	6000	0.573
4775	0.456	6000	0.524	6303	0.626
5381	0.5	6361	0.559	6606	0.696
6000	0.566	6715	0.598	6754	0.743

Table A-3. The B-737 Comprehensive Test Results (Continued)

Test 1		Test 2		Test 3	
Flights	Crack Length (in.)	Flights	Crack Length (in.)	Flights	Crack Length (in.)
6348	0.626	6982	0.636	6830	0.785
6582	0.673	7333	0.706	6897	0.839
6764	0.727	7433	0.752	6956	0.953
6873	0.791			6969	1.038
6945	0.85				
7013	0.985				
7017	1.029				
7022	1.14				

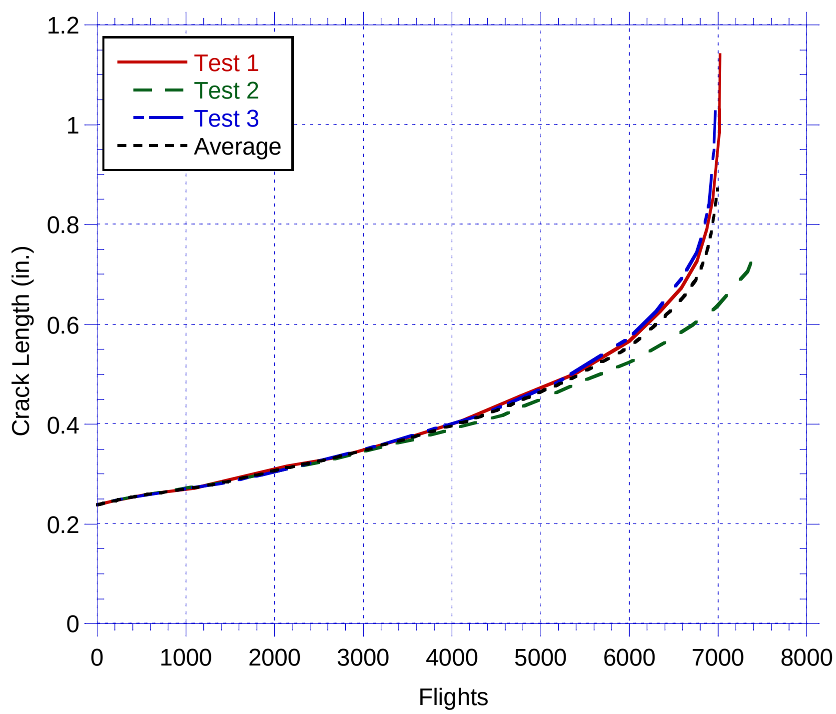

Figure A-6. The B-737 Comprehensive Test Results and Average Curve

Table A-4. The B-737 CA 1.3 Test Results

Test 1		Test 2		Test 3	
Flights	Crack Length (in.)	Flights	Crack Length (in.)	Flights	Crack Length (in.)
0	0.238	0	0.238	0	0.238
803	0.263	800	0.268	799	0.264
1600	0.288	1600	0.285	1599	0.288
2400	0.315	2600	0.31	2399	0.311
3200	0.349	3600	0.338	3201	0.346
4000	0.403	4600	0.379	4000	0.387
4599	0.446	5600	0.432	4602	0.427
5099	0.499	6500	0.512	5100	0.471
5549	0.573	7128	0.619	5600	0.536
5881	0.662	7433	0.731	5901	0.594
6108	0.784	7589	0.856	6199	0.685
6183	0.934	7642	1.397	6399	0.822
				6465	1.071

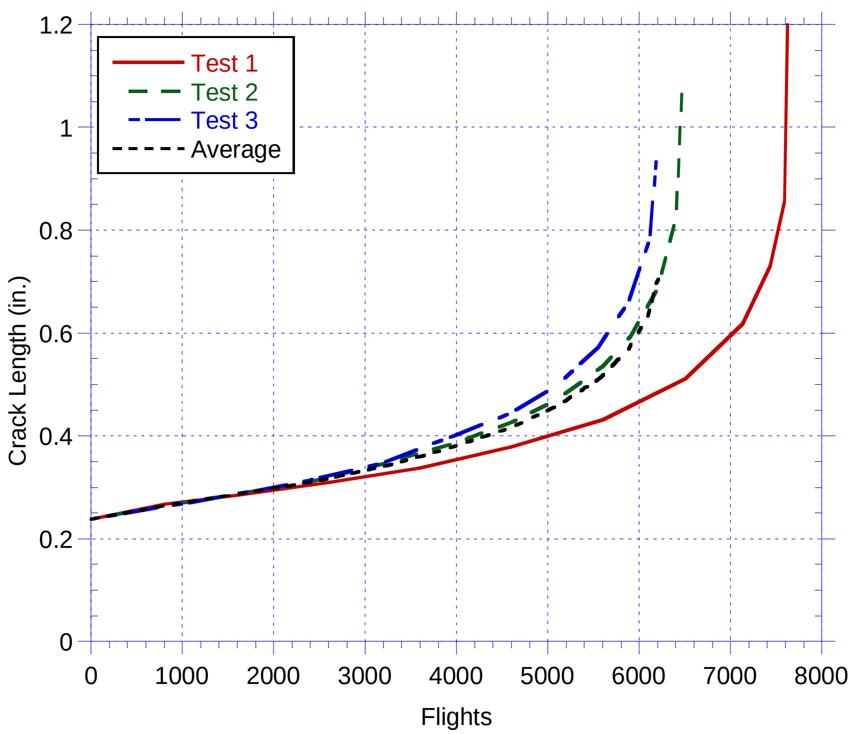

Figure A-7. The B-737 CA 1.3 Test Results and Average Curve

Table A-5. The B-777 Comprehensive Test Results

Test 1		Test 2		Test 3	
Flights	Crack Length (in.)	Flights	Crack Length (in.)	Flights	Crack Length (in.)
0	0.238	0	0.236	0	0.238
1106.3	0.289	517.85	0.265	737.56	0.279
1598.1	0.309	977.72	0.286	1106.3	0.298
2225.5	0.335	1598.1	0.307	1598.1	0.323
2857.4	0.371	2237.3	0.337	2237.3	0.357
3000	0.381	2640	0.358	2778.2	0.393
3456.3	0.413	3454.3	0.417	3081.8	0.419
4081.2	0.465	4081.2	0.466	3454.3	0.452
4398.6	0.503	4522.6	0.514	4017.5	0.505
4738.5	0.533	5138.4	0.582	4646.6	0.604
5125	0.576	5500	0.62	5048.6	0.678
5385.4	0.606	5675.3	0.66	5339.6	0.744
5609.6	0.649	6000	0.725	5492.8	0.809
5826.3	0.683	6173.3	0.769	5634.1	0.941
6000	0.725	6268	0.795	5698.9	1.014
6176	0.772	6357.2	0.841	5707.9	1.082
6296.3	0.819	6405.7	0.881		
6384.6	0.87	6454.8	0.953		
6441.2	0.921	6472	0.993		
6459.7	0.961	6481.9	1.026		
6474.9	0.989	6491.7	1.071		
6478.4	0.998	6501.4	1.138		
6489.7	1.025				
6498.5	1.062				
6508.4	1.121				

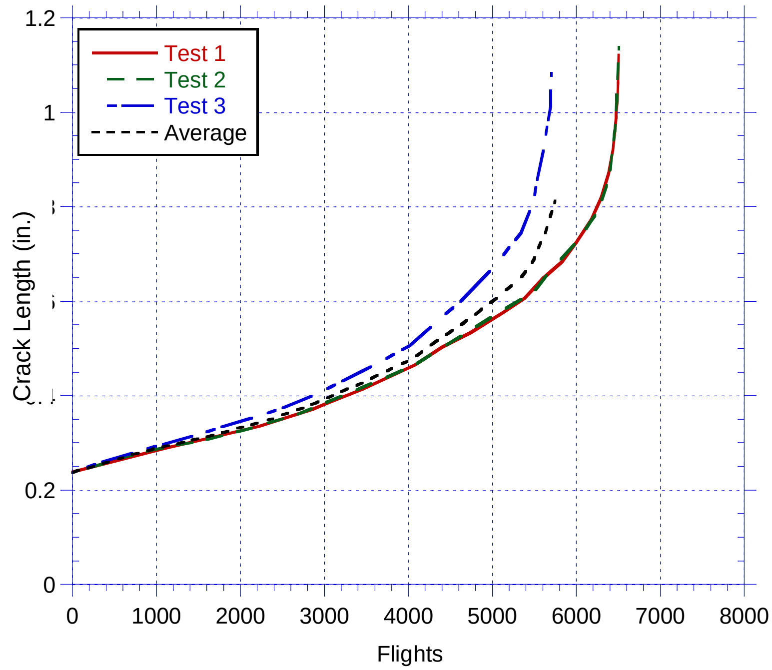

Figure A-8. The B-777 Comprehensive Test Results and Average Curve

Table A-6. The B-777 CA 1.3 Test Results

Test 1		Test 2		Test 3	
Flights	Crack Length (in.)	Flights	Crack Length (in.)	Flights	Crack Length (in.)
0	0.238	0	0.238	0	0.238
501	0.262	510	0.259	505	0.26
1015	0.281	1003	0.279	1001	0.28
1504	0.307	1521	0.305	1502	0.3
2009	0.332	2045	0.331	2003	0.331
2502	0.361	2513	0.365	2500	0.371
2972	0.396	2963	0.406	2962	0.419
3350	0.429	3356	0.448	3352	0.476
3713	0.464	3706	0.501	3699	0.543
4055	0.506	4000	0.556	3951	0.617
4351	0.549	4283	0.636	4073	0.666
4601	0.598	4491	0.715	4222	0.753
4821	0.65	4649	0.819	4368	0.918
5009	0.707	4736	0.923	4407	1.015

Table A-6. The B-777 CA 1.3 Test Results (Continued)

Test 1		Test 2		Test 3	
Flights	Crack Length (in.)	Flights	Crack Length (in.)	Flights	Crack Length (in.)
5193	0.784	4752	0.952		
5292	0.846	4771	1.001		
5373	0.915	4785	1.049		
5413	0.969				
5436	1.014				
5449	1.042				

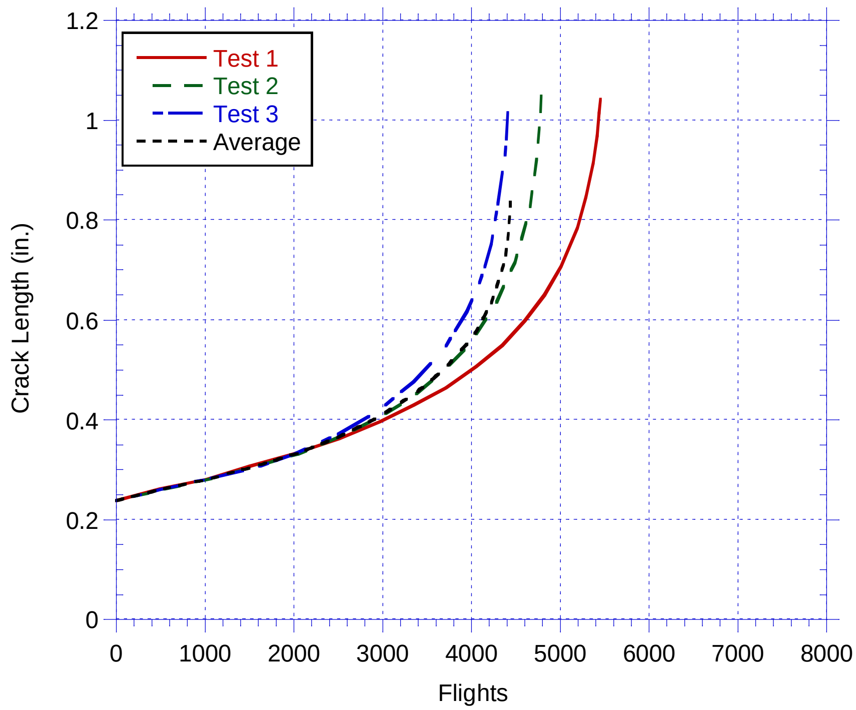

Figure A-9. The B-777 CA 1.3 Test Results and Average Curve

Table A-7. The B-777 CA 1.15 Test Results

Test 1		Test 2		Test 3	
Flights	Crack Length (in.)	Flights	Crack Length (in.)	Flights	Crack Length (in.)
0	0.238	0	0.238	0	0.238
597	0.253	606	0.254	600	0.258
1201	0.273	1199	0.273	1200	0.278
1801	0.293	1801	0.292	1800	0.296
2400	0.316	2400	0.317	2400	0.323
2999	0.345	3000	0.348	3000	0.351
3500	0.374	3501	0.378	3500	0.38
4000	0.41	4001	0.409	3999	0.408
4505	0.451	4400	0.447	4401	0.44
4995	0.505	4801	0.488	4799	0.48
5399	0.56	5201	0.537	5201	0.532
5701	0.614	5499	0.588	5499	0.593
5918	0.664	5751	0.637	5751	0.639
6124	0.727	5999	0.704	6001	0.725
6296	0.791	6199	0.773	6177	0.804
6476	0.903	6361	0.864	6332	0.931
6547	0.974	6432	0.927	6394	1.034
6568	1.062	6493	1.011	6426	1.128
6586	1.099	6517	1.058		
		6546	1.202		

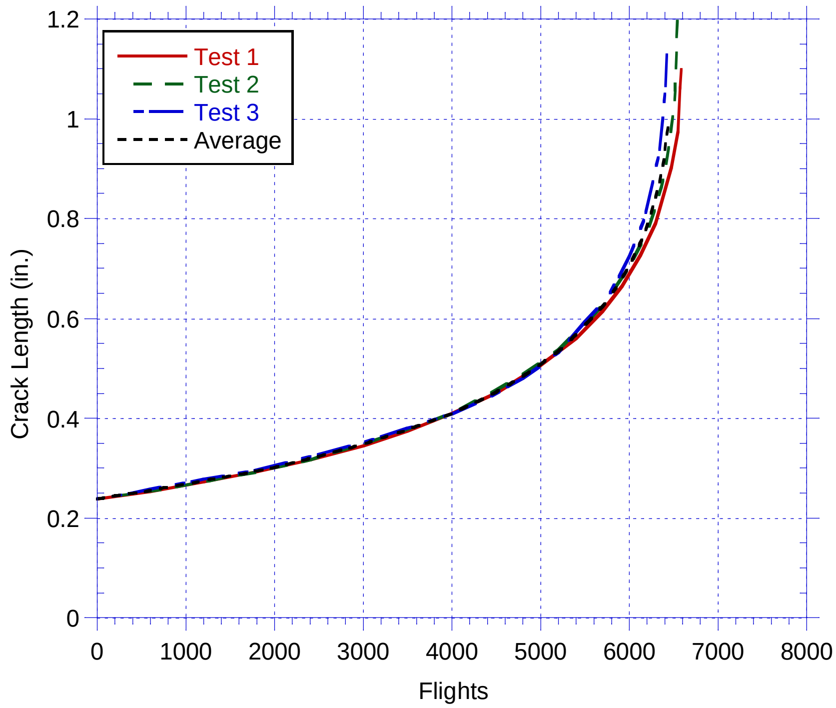

Figure A-10. The B-777 CA 1.15 Test Results and Average Curve

Table A-8. The B-777 CA 1.1 Sequence Test Results

Test 1		Test 2		Test 3	
Flights	Crack Length (in.)	Flights	Crack Length (in.)	Flights	Crack Length (in.)
0	0.238	0	0.238	0	0.238
599	0.26	600	0.255	600	0.255
1208	0.275	1204	0.27	1201	0.27
1800	0.294	1805	0.288	1800	0.291
2400	0.321	2400	0.307	2400	0.316
2999	0.353	3000	0.332	2999	0.344
3500	0.39	3499	0.356	3499	0.374
3901	0.423	3900	0.378	4052	0.415
4199	0.449	4199	0.394	4500	0.451
4500	0.481	4500	0.414	4900	0.491
4800	0.519	4801	0.435	5300	0.55
4999	0.549	5104	0.461	5599	0.598
5201	0.587	5400	0.487	5850	0.654
5399	0.636	5599	0.512	6048	0.709

Table A-8. The B-777 CA 1.1 Sequence Test Results (Continued)

Test 1		Test 2		Test 3	
Flights	Crack Length (in.)	Flights	Crack Length (in.)	Flights	Crack Length (in.)
5599	0.688	5799	0.53	6251	0.788
5809	0.774	5999	0.557	6390	0.873
5943	0.857	6201	0.586	6497	0.978
6034	0.946	6400	0.62	6549	1.075
6070	0.997	6600	0.659		
6098	1.061	6800	0.711		
6126	1.157	6965	0.76		
		7114	0.816		
		7232	0.88		
		7346	0.978		
		7372	1.012		
		7391	1.042		
		7405	1.075		

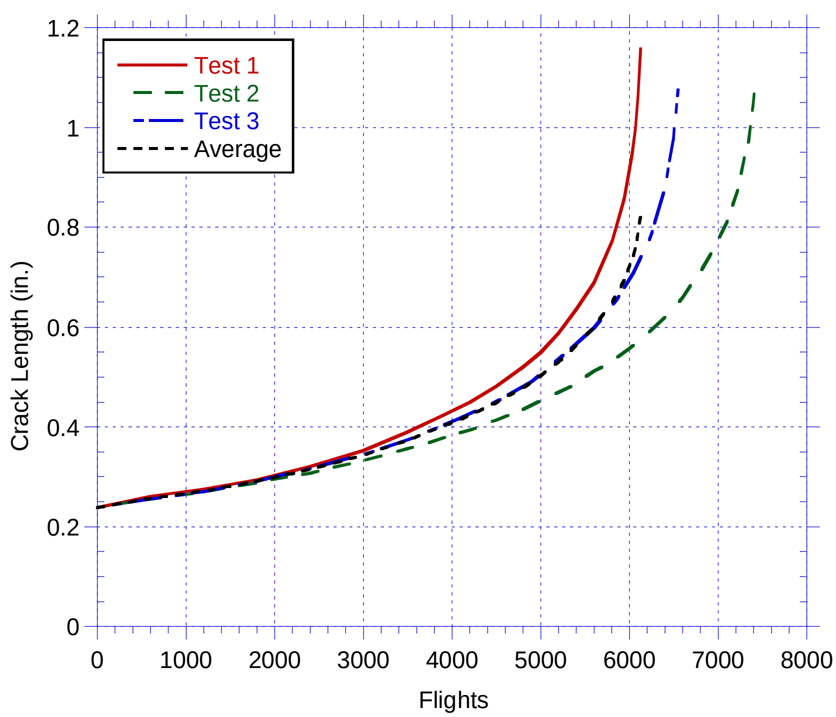

Figure A-11. The B-777 CA 1.1 Test Results and Average Curve

APPENDIX B—da/d$_{FLIGHT}$ AND DATA EDITING

1. DA/D$_{FLIGHT}$.

When the comprehensive sequence data were obtained, it was noted that for some tests, during the early stages of growth, the growth rate unexpectedly decreased instead of increasing. To further investigate this apparent anomaly, the crack growth rate per flight (da/d$_{Flight}$) was calculated as a function of crack length. Figures B-1 through B-16 show the results for the comprehensive and constant-amplitude sequence tests. These data are shown in figures B-1, B-6, and B-10 for the comprehensive sequence tests conducted for the ERJ-145, B-737, and B-777, respectively. It is also shown in figures B-4, B-8, B-12, B-14, and B-16 for constant-amplitude sequence tests. The largest initial decrease occurred for the ERJ-145 sequence on test number 1 (see figure A-1). However, the trend was not always present and the magnitude varied significantly when present. It was also noted that by the time the half-crack length was approximately 0.375″, the nominal rate was increasing in a relatively stable manner for all tests conducted. The cause of the initial decrease was not investigated any further. For the purpose of this effort, it was decided to discard all crack growth data collected prior to a half-crack length of 0.375″ for all sequences before comparing the results.

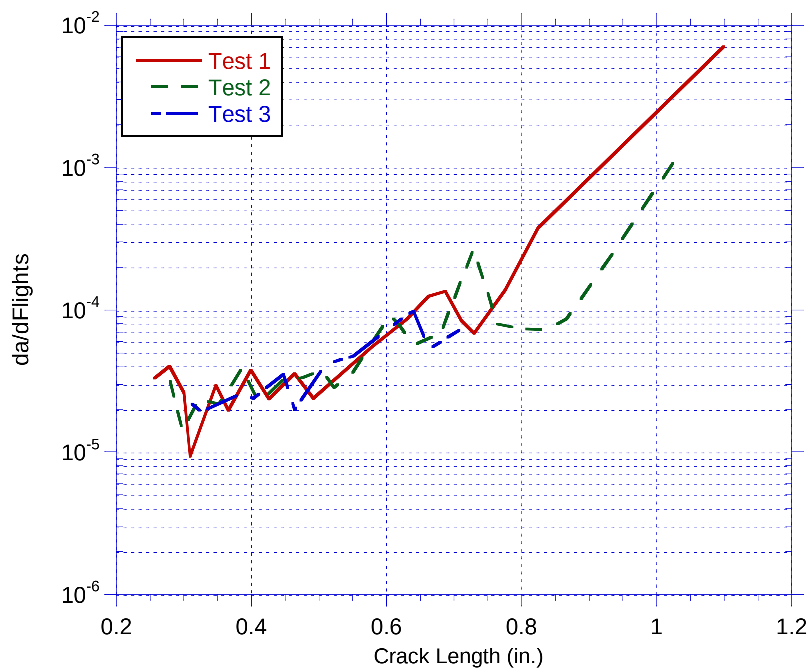

Figure B-1. The ERJ-145 Comprehensive Sequence da/d$_{Flight}$ vs Crack Length

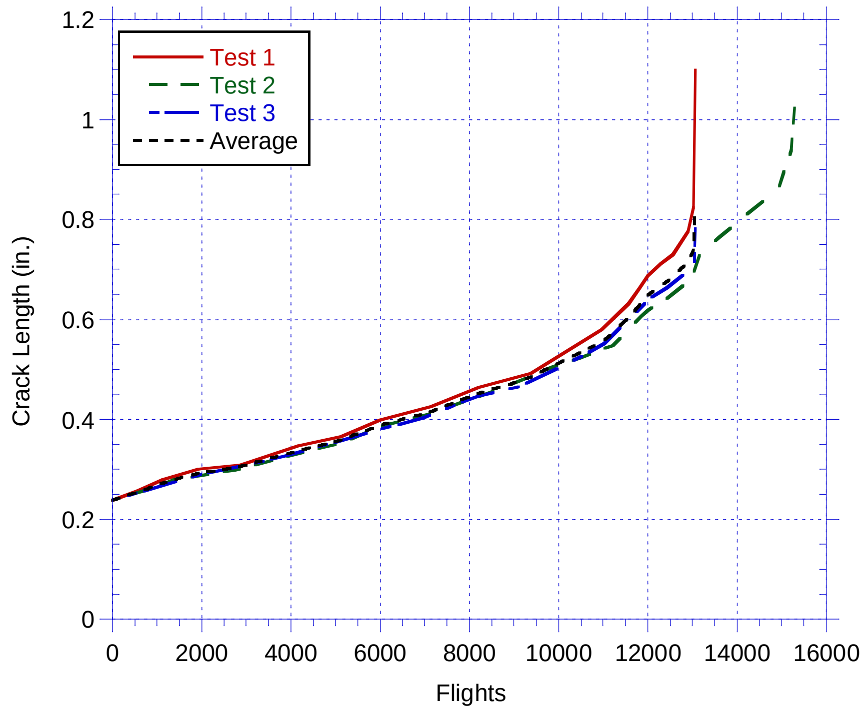

Figure B-2. ERJ-145 Comprehensive Sequence Crack Growth Curves

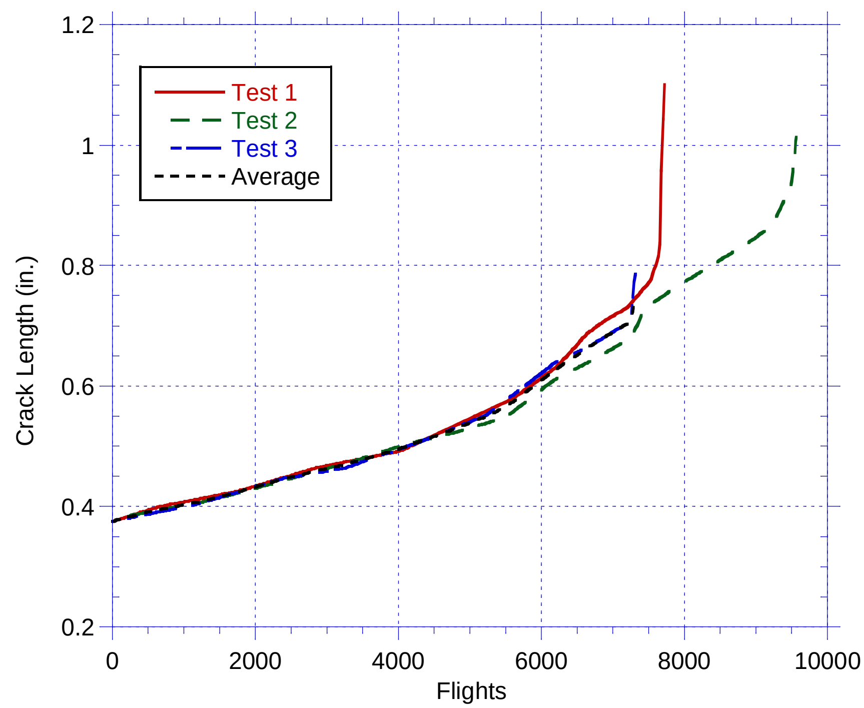

Figure B-3. Edited ERJ-145 Comprehensive Sequence Crack Growth Curves

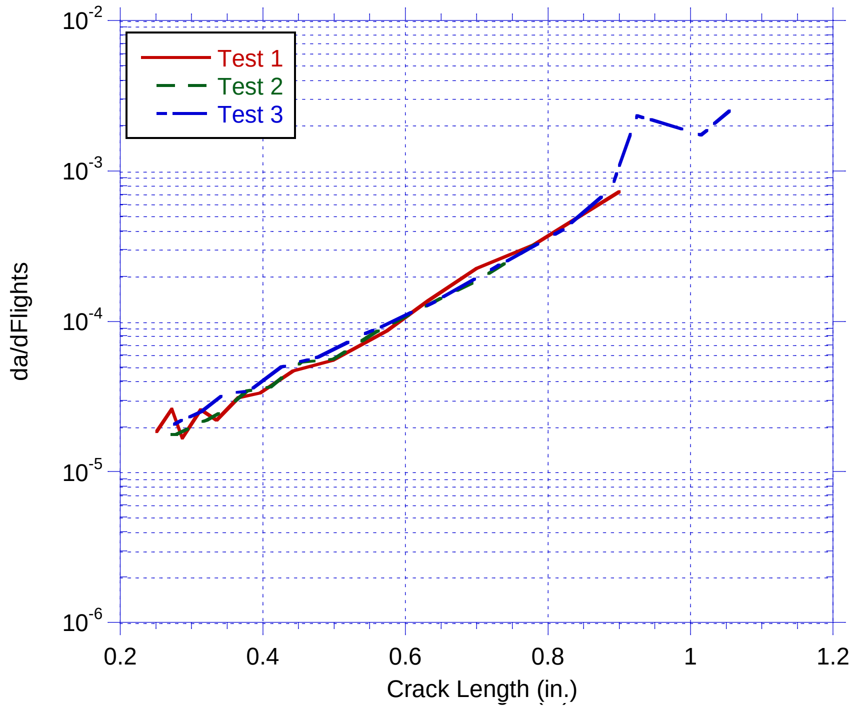

Figure B-4. The ERJ-145 CA 1.3 Sequence da/d$_{Flight}$ vs Crack Length

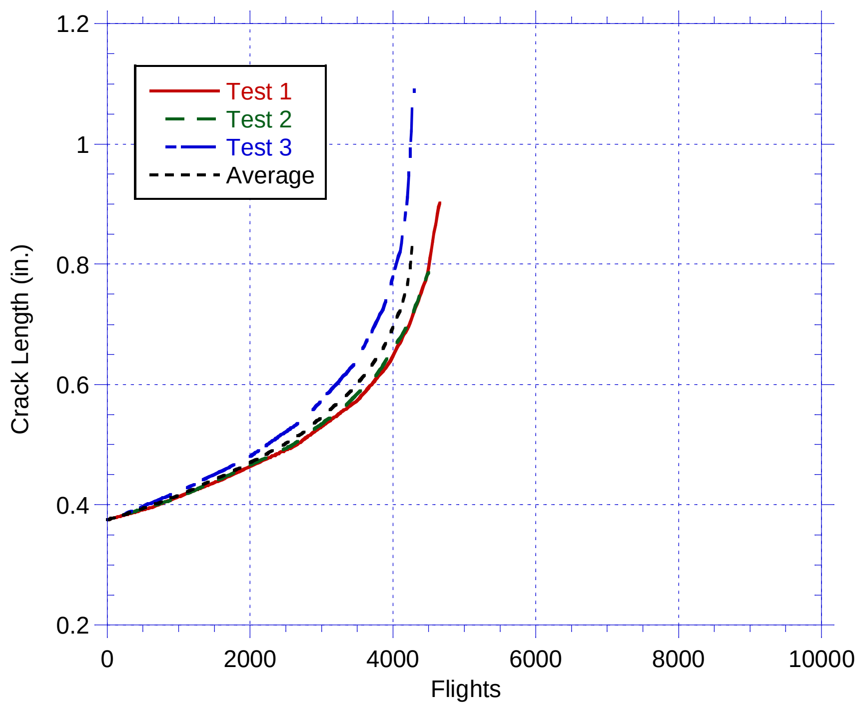

Figure B-5. Edited ERJ-145 CA 1.3 Sequence Crack Growth Curves

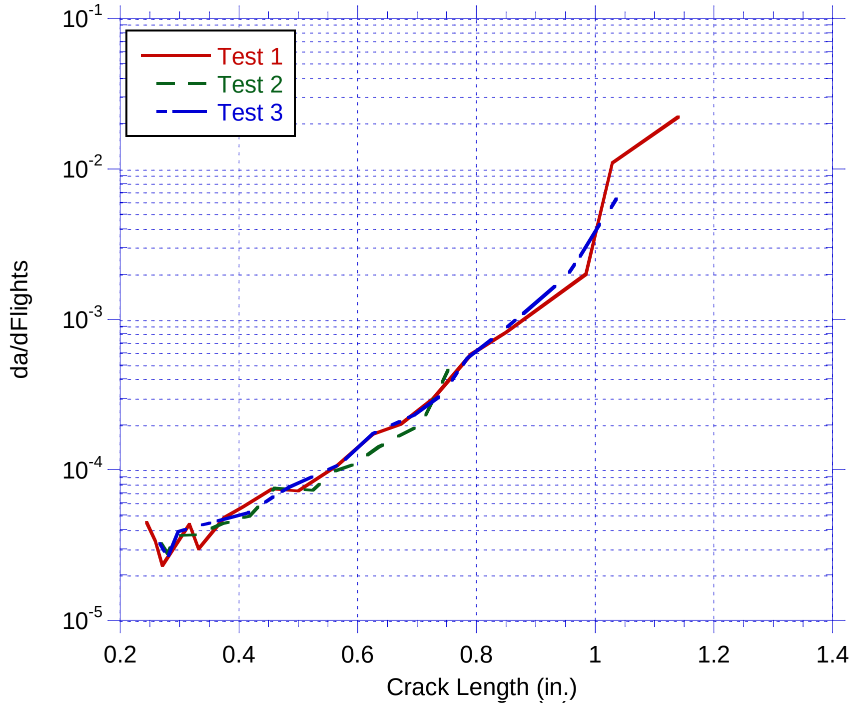

Figure B-6. The B-737 Comprehensive Sequence da/d$_{\text{Flight}}$ vs Crack Length

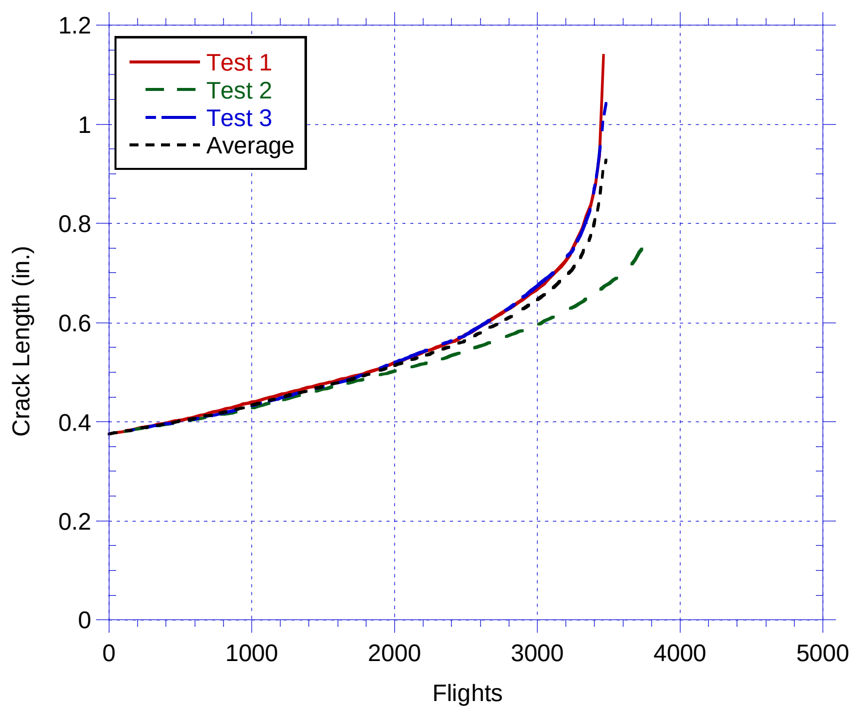

Figure B-7. Edited B-737 Comprehensive Sequence Crack Growth Curves

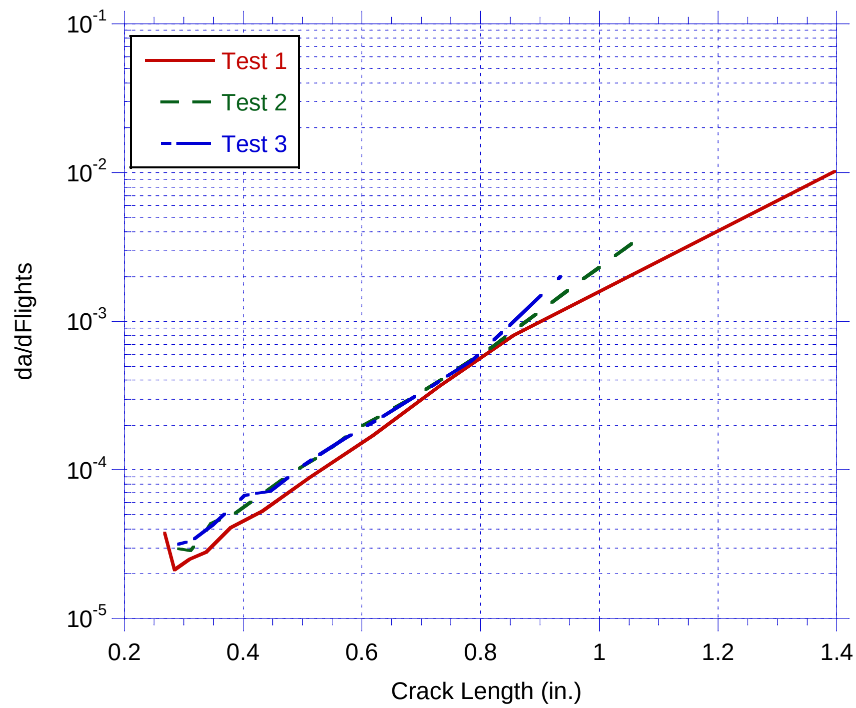

Figure B-8. The B-737 CA 1.3 Sequence da/d$_{Flight}$ vs Crack Length

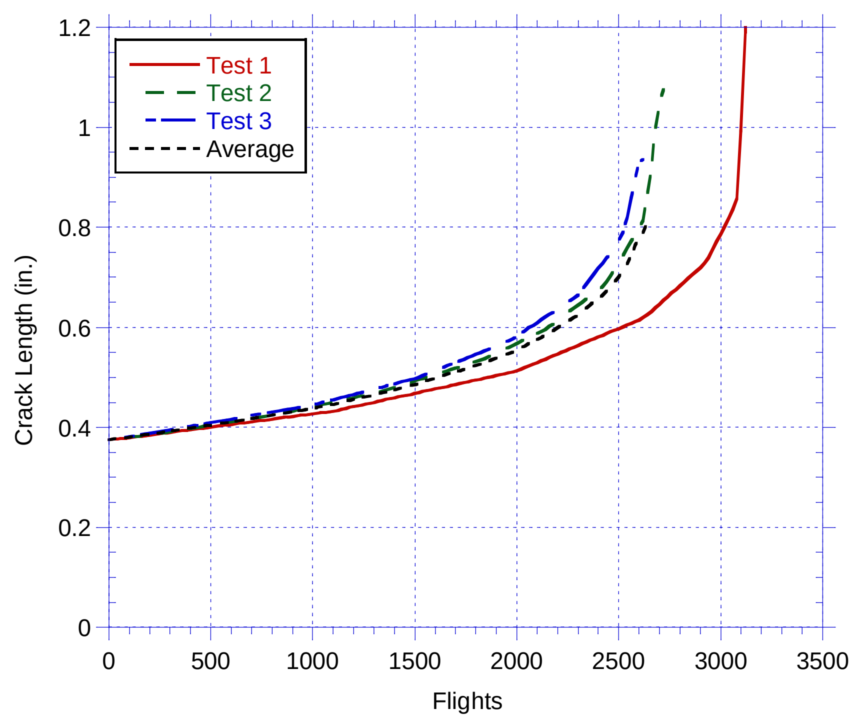

Figure B-9. Edited B-737 CA 1.3 Sequence Crack Growth Curves

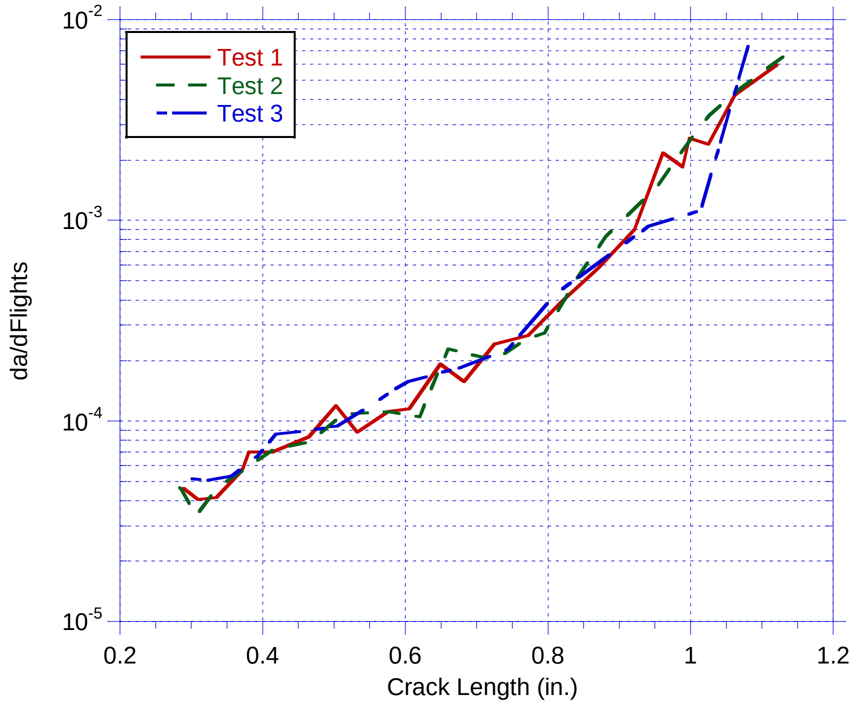

Figure B-10. The B-777 Comprehensive Sequence da/d_{Flight} vs Crack Length

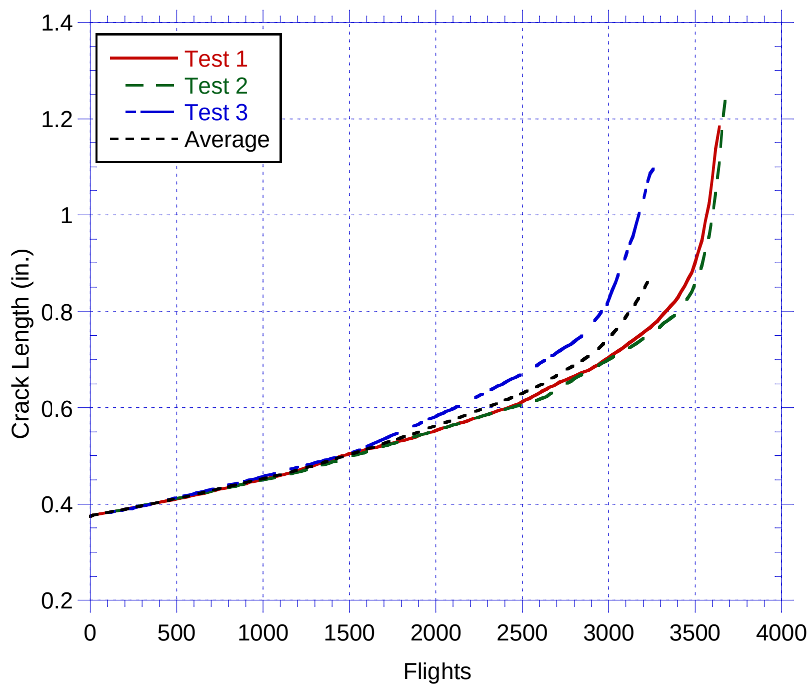

Figure B-11. Edited B-777 Comprehensive Sequence Crack Growth Curves

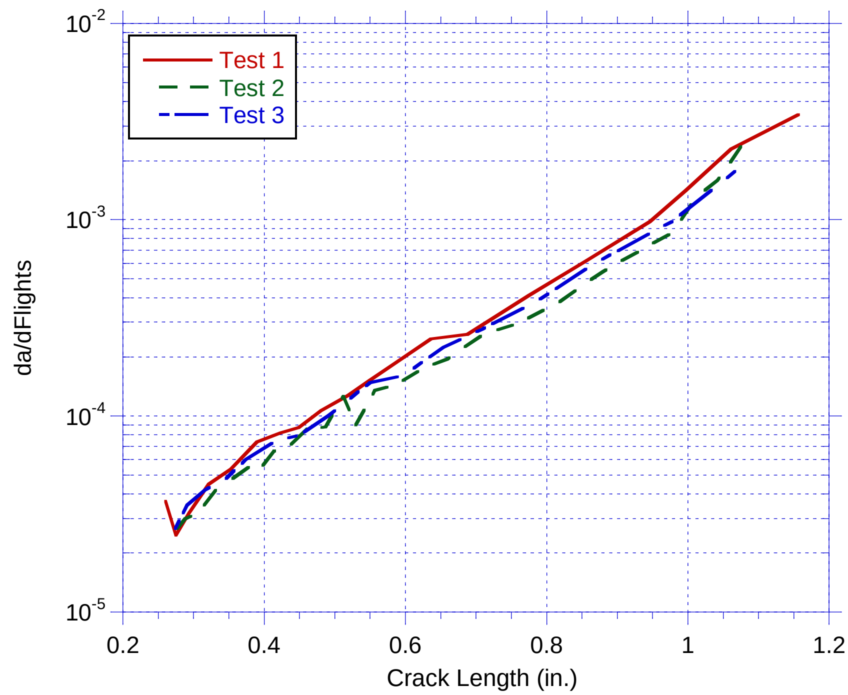

Figure B-12. The B-777 CA 1.1 Sequence da/d$_{\text{Flight}}$ vs Crack Length

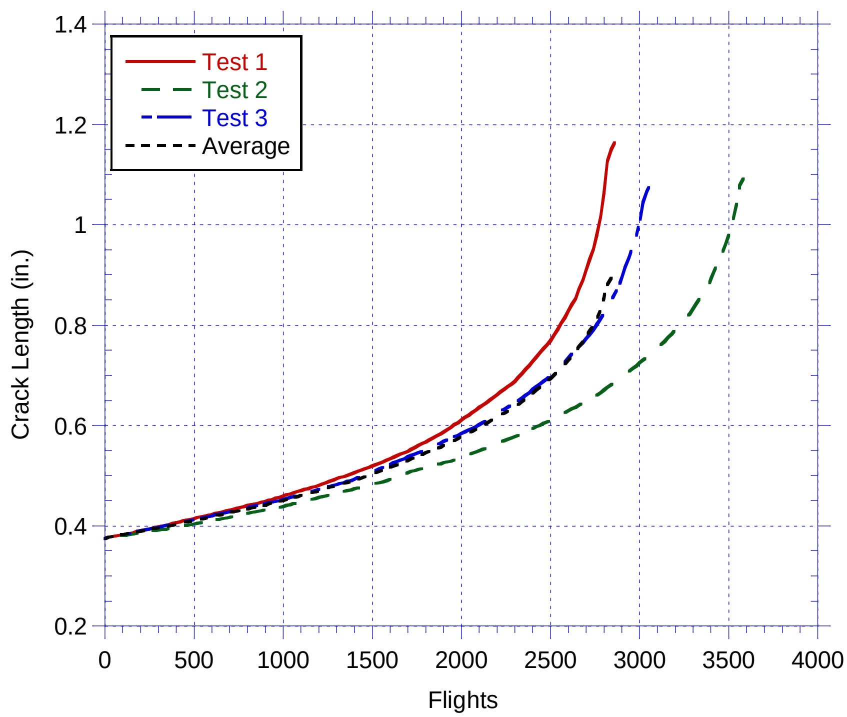

Figure B-13. Edited B-777 CA 1.1 Sequence Crack Growth Curves

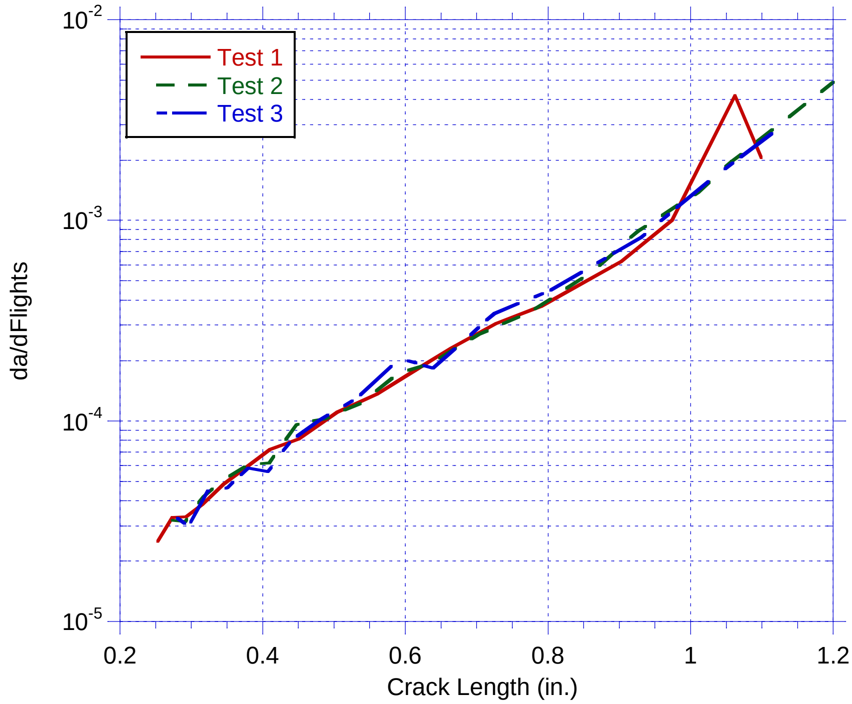

Figure B-14. The B-777 CA 1.15 Sequence da/d_{Flight} vs Crack Length

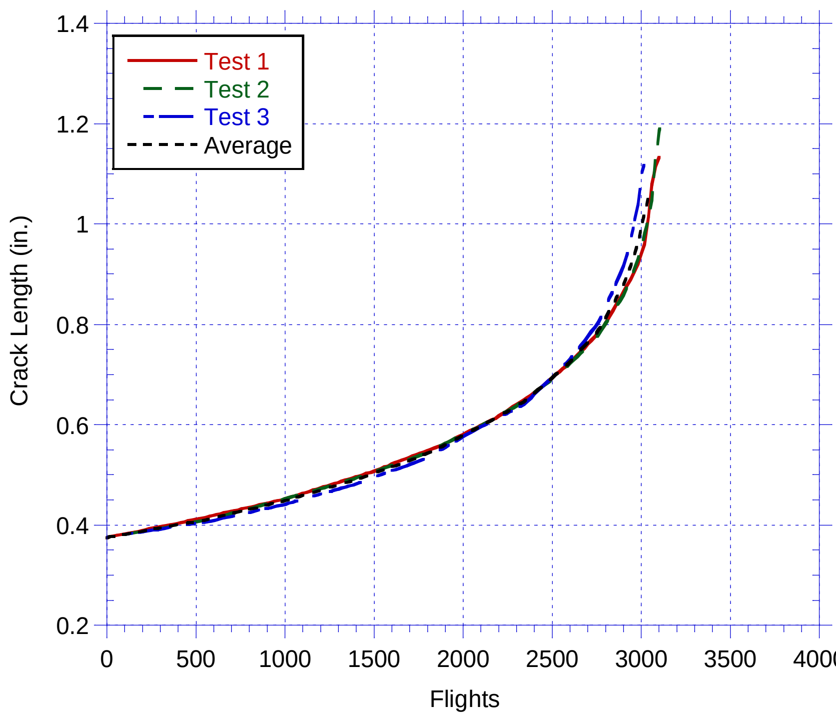

Figure B-15. Edited B-777 CA 1.15 Sequence Crack Growth Curves

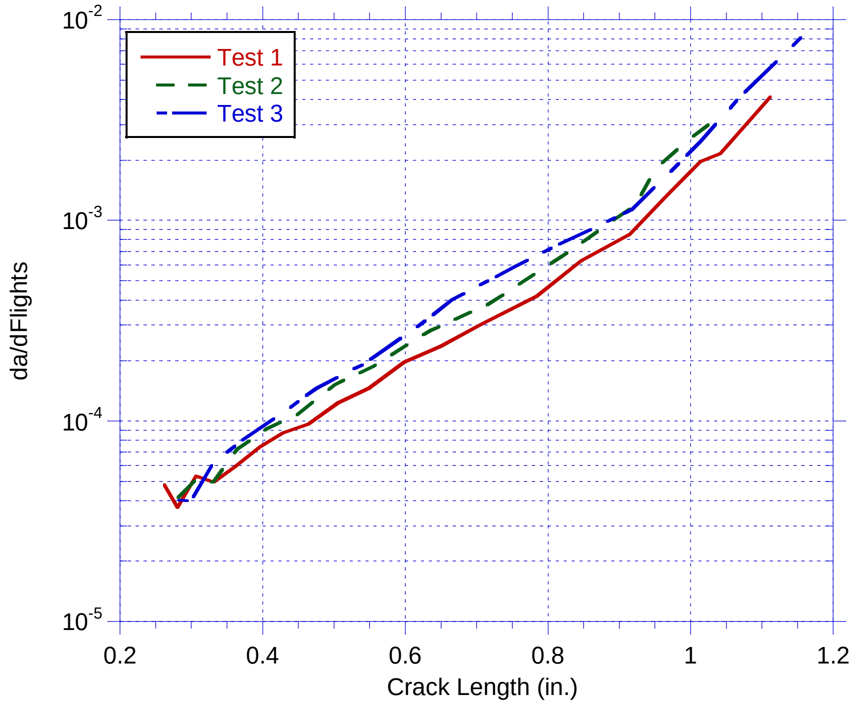

Figure B-16. The B-777 CA 1.3 Sequence da/d$_{Flight}$ vs Crack Length

2. DATA EDITING.

The crack growth up to the 0.375″ half-crack length was omitted from all test results and crack growth as a function of flights was replotted. Following this, an average crack growth curve was generated from the three tests for each comprehensive and constant-amplitude sequence. The resulting curves are shown in figures B-3, B-5, B-7, B-9, B-11, B-13, and B-17. The average curves were used for the results presented in section 6.5 of the main report.

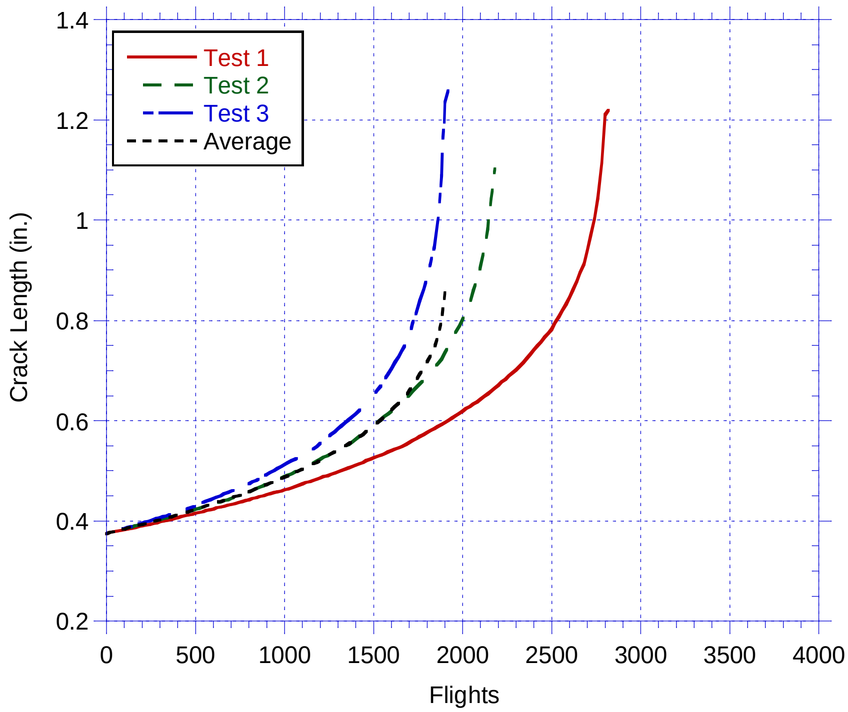

Figure B-17. Edited B-777 CA 1.3 Sequence Crack Growth Curves